Influences on Observed Near-Surface Gust Factors in Landfalling U.S. Gulf Coast Hurricanes: 2004–08

IAN M. GIAMMANCO,[a,b] JOHN L. SCHROEDER,[c] FORREST J. MASTERS,[d] PETER J. VICKERY,[e] RICHARD J. KRUPAR III,[b,f] AND JUAN-ANTONIO BALDERRAMA[d]

[a] *Insurance Institute for Business and Home Safety, Richburg, South Carolina*
[b] *National Wind Institute, Texas Tech University, Lubbock, Texas*
[c] *Department of Geosciences, Texas Tech University, Lubbock, Texas*
[d] *Department of Civil and Environmental Engineering, University of Florida, Gainesville, Florida*
[e] *Applied Research Associates, Raleigh, North Carolina*
[f] *School of Civil Engineering, University of Queensland, St. Lucia, Queensland, Australia*

(Manuscript received 25 January 2016, in final form 19 September 2016)

ABSTRACT

The deployment of ruggedized surface observing platforms by university research programs in the path of landfalling tropical cyclones has yielded a wealth of information regarding the near-surface wind flow characteristics. Data records collected by Texas Tech University's Wind Engineering Mobile Instrument Tower Experiment and StickNet probes and by the Florida Coastal Monitoring Program along the Gulf Coast of the United States from 2004 to 2008 were compiled to examine influences on near-surface gust factors. Archived composite reflectivity data from coastal WSR-88D instruments were also merged with the tower records to investigate the influence of precipitation structure. Wind records were partitioned into 10-min segments, and the ratio of the peak moving-average 3-s-gust wind speed to the segment mean was used to define a gust factor. Observations were objectively stratified into terrain exposure categories to determine if factors beyond those associated with surface frictional effects can be extracted from the observations. Wind flow characteristics within exposure classes were weakly influenced by storm-relative position and precipitation structure. Eyewall observations showed little difference in mean gust factors when compared with other regions. In convective precipitation, only peak gust factors were slightly larger than those found in stratiform conditions, with little differences in the mean. Gust factors decreased slightly with decreasing radial distance in rougher terrain exposures and did not respond to radar-observed changes in precipitation structure. In two limited comparisons, near-surface gusts did not exceed the magnitude of the wind maximum aloft detected through wind profiles that were derived from WSR-88D velocity–azimuth displays.

1. Introduction

Since 1998, university research programs have deployed ruggedized weather monitoring systems into the path of U.S. landfalling tropical cyclones to measure near-surface winds. These data represent a large percentage of the complete wind records from the most notable U.S. landfalls over the past 15 years. Conventional observing stations do not provide the high-resolution observations needed to examine the turbulent properties of tropical cyclone wind flows, and failure rates approach 80% when peak 3-s gust wind speeds exceed $32\,m\,s^{-1}$, most often because of loss of electrical power (Blessing and Masters 2005). The deployment of research-driven observing systems in the path of landfalling tropical cyclones by U.S. universities has been crucial to the documentation and characterization of tropical cyclone winds over land. The current study examines the observations of near-surface gust factors from high-resolution archived wind records collected by Texas Tech University (TTU) and the Florida Coastal Monitoring Program (FCMP) from landfalling U.S. Gulf Coast hurricanes from 2004 to 2008 (Schroeder and Smith 2003; Yu et al. 2008; Masters et al. 2010).

The combined archive contains more than 90 complete high-resolution (sampling rate ≥ 1 Hz) wind records. The study presented here uses 10-m observations obtained by FCMP and TTU's Wind Engineering Mobile Instrument Tower Experiment (WEMITE) and

Corresponding author e-mail: Ian M. Giammanco, igiammanco@ibhs.org

DOI: 10.1175/JAMC-D-16-0053.1

2.25-m observations from TTU's StickNet adaptive observing network (Schroeder and Smith 2003; Weiss and Schroeder 2008; Masters et al. 2010; Balderrama et al. 2011). Influences on the observed gust factors associated with changes in upstream terrain exposure and larger-scale dynamical and precipitation processes are investigated to build upon the work of Schroeder et al. (2009) and Masters et al. (2010) through the use of this sizeable dataset.

Historical literature has shown that turbulence in the hurricane boundary layer (HBL) is primarily governed by mechanical mixing due to upstream terrain elements that produce a well-mixed and neutrally stratified boundary layer. It is well understood that large changes to the wind flow characteristics within a single time history are a result of changes in fetch and subsequent differences in the upstream terrain (Vickery and Skerlj 2005; Paulsen and Schroeder 2005; Schroeder et al. 2009). The research tower deployments that make up the archive used in this study often targeted relatively uniform terrain exposure locations (i.e., airports). As identified by Powell et al. (2004), these locations are often not uniform in exposure across all directions and are not necessarily representative of standard open-terrain conditions. Transitional flow regimes, where the flow may not be in equilibrium with the underlying terrain, are also contained within data records. To determine if factors beyond terrain conditions affect gust factors, objective stratification of the observations is required (Krayer and Marshall 1992; Sparks and Huang 2001; Schroeder and Smith 2003; Paulsen and Schroeder 2005; Vickery and Skerlj 2005; Yu et al. 2008; Schroeder et al. 2009; Harper et al. 2010; Miller et al. 2015).

Past research often evaluated differences in gust factors between those in tropical cyclone winds and those produced by land-based convection and large-scale synoptic systems. The results were important in understanding differences in wind climate and how they may influence minimum structural design standards (Krayer and Marshall 1992; Sparks and Huang 2001; Schroeder and Smith 2003; Paulsen and Schroeder 2005; Vickery and Skerlj 2005; Yu et al. 2008). Gust factors have been observed to show some influence from processes not associated with upstream terrain in various environments. Vickery and Skerlj (2005) identified a slight decrease in gust factors as mean winds increased. A more recent study by Schroeder et al. (2009) observed a more pronounced reduction in hurricane gust factors with increasing mean wind speed. The result was attributed to the inclusion of more observations from higher wind speed regimes, which previous studies had lacked. Additionally, a radial dependence was found with regard to mean gust factors and mean longitudinal integral length scales. The study also coupled wind measurements with WSR-88D reflectivity data and found a slight increase in gust factors for periods of more intense precipitation. The presence of deeper vertical mixing could lead to a more effective transport of higher momentum to the surface, and Powell et al. (2003) hypothesized that the maximum aloft represents the upper bound of near surface. Applying this hypothesis to the mechanisms described by Kepert (2001), Kepert and Wang (2001), and Schwendike and Kepert (2008) supports the premise that factors beyond upstream terrain could contribute to the near-surface wind flow characteristics.

Extreme wind gusts and large gust factors beyond what would be anticipated for the underlying upstream terrain have been documented during Hurricane Hugo (1989), Cyclone Orson (1989), Hurricane Andrew (1992), Hurricane Bertha (1996), and Cyclone Olivia (1996). The notable gusts were largely attributed to transient convective-scale features or eyewall mesovortices (Powell et al. 1991, 1996; Marks et al. 2008; Harper et al. 2010). The literature frequently mentions the possibility that extreme gusts are produced by mesoscale features and/or convective processes (e.g., Fujita 1985; Ashcroft 1994; Sparks and Huang 2001; Schroeder and Smith 2003; Bradbury et al. 1994; Paulsen and Schroeder 2005; Vickery and Skerlj 2005). Fujita (1985, 1992) speculated that buoyancy-driven downbursts could contribute to large surface gusts and an increase in damage. The hypothesis is countered by the more recent results of Suomi et al. (2015), which found little difference between gust factors in neutral and convectively unstable boundary layers, and the lack of near-surface observations successfully capturing the features on land (Sparks and Huang 2001; Vickery and Skerlj 2005; Schroeder et al. 2009; Masters et al. 2010).

Deep convection in a tropical cyclone is typically found in cellular structures in outer rainbands and the eyewall region (Jorgensen 1984). Unlike land-based convection, vertical velocities rarely exceed $15\,m\,s^{-1}$ and the vertical momentum fluxes are an order of magnitude smaller (Black et al. 1996; Eastin et al. 2005). Within the rainband regions, where convectively induced gusts may be more prevalent, large gust factors as they relate to damage potential may be of less importance. The relatively low mean wind environment, when compared with that of the eyewall, means that peak wind gust magnitudes are unlikely to exceed those of the eyewall region. It is unclear if buoyancy-driven gusts within the eyewall can produce gust factors that deviate from those generated purely from mechanical turbulence. Recent observational studies argued that these types of gusts are difficult to distinguish from those

produced through mechanical mixing in either the eyewall or outer-vortex regions (Schroeder et al. 2009; Masters et al. 2010; Miller et al. 2015).

Smaller-scale coherent features have also been observed in the HBL. The presence of rolls and/or streaks has been found to augment the near-surface wind flow characteristics (Wurman and Winslow 1998; Morrison et al. 2005; Lorsolo et al. 2008; Kosiba et al. 2013; Kosiba and Wurman 2014). The depth of such features could enhance the downward transport of higher momentum associated with the wind maximum aloft. Lorsolo et al. (2008) and Kosiba and Wurman (2014) examined subkilometer features and their effect on the near-surface wind flow. The results indicated that perturbations associated with roll or streak structures are typically not large enough to result in anomalous gusts within their respective terrain exposure. There has been some preliminary evidence using mobile research radars to suggest that similar features may exist in other nontropical cyclone wind regimes (i.e., thunderstorm outflow or synoptically driven wind events). It is postulated that the near-surface flow organizes into coherent features as mean winds increase in many different environments, which also supports evidence shown by Suomi et al. (2015) (J. Schroeder 2015, personal communication). It is noted that, if confirmed, the influence of these structures are likely represented within observed gust factor distributions.

2. Data and methodology

The present study examines observations of near-surface gust factors grouped by surface roughness length z_o to determine if influences beyond those associated with upstream terrain can be extracted and are meaningful. For the purposes of this study, comparisons with theoretical wind spectra and different time-averaging techniques will not be included. These topics are covered in detail by Harper et al. (2010), which provides a robust reference to explain how these factors affect the measurement of near-surface wind flow characteristics. The reader is referred to this work for conversion tables between averaging times and observing standards, as they fall outside of the scope of this study.

Observations are first separated by measurement height (10-m height for WEMITE and FCMP platforms and 2.25 m for StickNet probes). Data records are segmented using a 10-min window to calculate the wind flow characteristics (e.g., longitudinal turbulence intensity, gust factor, and longitudinal integral length scale). For the purposes of this study, only analyses of gust factors are included. The gust factor is defined as the ratio of the peak 3-s gust, determined by a moving average, to the 10-min mean wind speed of the data segment.

a. Instrumentation

Wind measurements by TTU WEMITE platforms are made at multiple levels from two ruggedized towers (WEMITE 1 and WEMITE 2) using propeller-vane anemometers. Gill propeller vertical wind component measurements were available at 10-m height for select deployments. Three additional portable meteorological towers (PMT) were also deployed. The platforms were 10-m towers with a single-level propeller-vane anemometer. The WEMITE and PMT platforms were used by TTU through 2006. The FCMP uses a fleet of six 10-m ruggedized, trailer-mounted towers that also collect wind data at multiple levels. The wind direction data collected by WEMITE and PMT platforms are recorded in a tower-relative coordinate system. During post-processing, the raw tower-relative wind direction data are rotated to a magnetic north–relative coordinate system by applying the known offset. The orientation of each tower is sighted by a compass at the onset of each deployment. For FCMP towers, the three-axis Gill instrument is oriented at 45° to the tower boom arm. Collected data are segmented into 10-min time histories in order to adjust the data into a coordinate system aligned with the mean flow and correct for tower tilt. Negligible mean vertical and lateral wind components for all platforms are verified to satisfy the requirements of an eddy-covariance method of analysis (Stull 1988).

In 2007, TTU transitioned to StickNet probes, which are 2.25-m, rapidly deployable surface observing stations (Weiss and Schroeder 2008). Two primary wind instrumentation configurations were employed from 2007 to 2011. Twelve probes used a conventional propeller-vane anemometer as their wind sensing device while the remaining used a two-dimensional sonic anemometer (Weiss and Schroeder 2008). The full fleet was converted to propeller-vane anemometers in 2011. StickNet wind direction data are output in a magnetic north–relative coordinate system through the use of an onboard electronic compass that determines probe orientation and the data acquisition system adjusts the wind direction accordingly.

The nonstandard measurement height of TTU StickNet probes warranted investigation of the differences in the turbulence quantities between measurements made at lower heights (2.5 m) and those made at 10 m. Mahrt et al. (2001) found differences in calculated z_o at different measurement heights and changes in the turbulence quantities as wind speeds increased within the same

TABLE 1. List of available 10-min data segments for each landfalling tropical cyclone and program.

Hurricane	Saffir–Simpson category at landfall	Program	No. of platforms	10-min data segments available
Ivan (2004)	3	FCMP	3	282
Ivan (2004)	3	TTU-WEMITE, PMT	4	620
Charley (2004)	4	FCMP	2	76
Dennis (2005)	3	FCMP	3	414
Katrina (2005)[a]	3	FCMP	3	335
Katrina (2005)[a]	3	TTU-WEMITE, PMT	3	465
Rita (2005)	3	FCMP	3	320
Rita (2005)	3	TTU-WEMITE, PMT	4	696
Dolly (2008)	1	TTU-StickNet	22	4491
Gustav (2008)	2	FCMP	4	384
Gustav (2008)	2	TTU-StickNet	19	3221
Ike (2008)	2	FCMP	5	618
Ike (2008)	2	TTU-StickNet	23	3411

[a] Saffir–Simpson category for Hurricane Katrina's final landfall in Mississippi.

stability regime. It was hypothesized that the streamlining of local vegetation may influence the wind flow characteristics and surface roughness estimates from observations closer to the ground with no change in upstream fetch (Mahrt et al. 2001). The turbulence intensities from several tropical cyclones using the 2.5- and 10-m observing levels of the WEMITE platforms exhibited a linear relationship (not shown). Higher values were observed at the lower level, as expected. The turbulence intensity (TI) method described by Beljaars (1987) was applied to WEMITE observations to estimate z_o. The calculated values from the two heights exhibited differences beyond those attributed to the logarithmic change in wind with height. The calculated z_o values from 2.5-m observations were then used to estimate the 10-m wind speed (no standardization to a common exposure), and differences between the two were identified. Interestingly, when the z_o value calculated from 10-m observations was used to standardize the 2.5-m wind observations to 10 m, the error was greatly reduced. The result raised issues in directly relating z_o values at the two heights using the TI method. For this study, the 2.25-m observations were still segregated by same z_o bins as 10-m observations. It is noted that the calculated z_o values may represent an "effective" roughness rather than the true underlying terrain. The results from the two measurement heights are presented separately because the focus is on determining if influences beyond frictional effects can be extracted from the observations.

b. *Quality control*

Each high-resolution time history was subjectively reviewed to ensure its general quality. Wind records were also subjected to a range test. Observations that fell outside ±3 standard deviations of a 1-min segmented mean inside each 10-min window were flagged for further scrutiny. Each 10-min segment of data was then subjected to a nonparametric run test with a 95% confidence interval requirement to ensure there was no significant trend within the window (Schroeder et al. 2009). Following the quality control procedures, 3590 10-min data segments at 10-m height and 11 123 data segments for 2.25-m observations were available for analysis. Of the data segments removed due to insufficient stationarity (128 at 10 m and 587 at 2.25 m) most were found in regions near outer rainbands at radii greater than 100 km. Table 1 provides a list of the landfalling tropical cyclones sampled and the available number of quality controlled 10-min data segments.

c. *Turbulence intensity method and roughness segregation*

To demonstrate the influence of upstream terrain as well as to identify changes beyond frictional effects, data segments were placed into the four terrain exposure categories used by Schroeder et al. (2009) (Table 2) based on calculated z_o. Within each roughness classification, additional stratifications were made to investigate the influence of mean wind speed, radial distance from the storm center, and precipitation structure. Surface roughness lengths for each 10-min data segment were computed using the TI method, which assumed neutral stratification and logarithmic wind profile and a constant ratio of frictional velocity u_* to the standard deviation of the longitudinal wind component ($\sigma_u/u_* = \text{constant}$; Beljaars 1987). The method was used due to instrumentation limitations on TTU WEMITE and StickNet platforms. The FCMP towers have the necessary instrumentation to calculate the true ratio and an eddy-covariance z_o (Stull 1988). These data were used to examine the influence this assumption has on the classifications and subsequent gust factor statistics.

TABLE 2. Roughness categories according to Schroeder et al. (2009) and total 10-min data segments for each.

Roughness regime	Roughness length (z_o; m)	Total 10-m data segments	Total 2.25-m data segments
Smooth	$0.005 \leq z_o \leq 0.0199$	949	5082
Open	$0.02 \leq z_o \leq 0.0499$	956	1845
Roughly open	$0.05 \leq z_o \leq 0.1899$	537	699
Rough	$0.19 \leq z_o \leq 0.5$	460	43

The FCMP data records were used to compute the actual value of σ_u/u_*, and u_* is defined through the classic eddy-covariance methodology by

$$u_* = [(\overline{u'w'})^2 + (\overline{v'w'})^2]^{1/4}. \quad (1)$$

The roughness length is then calculated for each 10-min segment, assuming neutral stability, by

$$z_o = z \exp\left(\frac{-k\overline{U}_z}{u_*}\right), \quad (2)$$

where z is the measurement height, k is the von Kármán constant (0.4), u_* is from Eq. (1), and $\overline{U}_z$ is the mean wind at height z (Stull 1988). The ratio σ_u/u_* from FCMP observations ranged from 1.78 to 3.15, with a mean of 2.95, which was in general agreement with those found by Miller et al. (2015) using a similar dataset (2.00–2.98). However, Miller et al. (2015) noted that the ratio may not be constant within the same wind record and general upstream fetch. Roughness lengths were also computed using the TI method using different ratios from 2.10 to 2.90, at values incrementally increasing by 0.1, to examine the sensitivity of the method to the ratio. The difference between the two estimates was also examined with respect to the 10-min mean wind speed (Fig. 1). At mean winds below 15 m s^{-1}, the differences between the two methods were large but decreased and converged as mean winds increased. When winds exceeded 20 m s^{-1}, the mean differences fell below 0.005 m and were smallest with an assumed ratio of 2.40. When observed gust factors over the range of z_o values from Table 1 were considered as a function of z_o, the slopes of the two log-linear trend lines were different. A shift toward smoother values and smaller gust factors was found for the TI method relationship at the assumed ratios below 2.50 (Fig. 2). The bias became less apparent above 2.50 and the best agreement found between the two curves used a constant of 2.70. FCMP observations were also placed into their respective terrain classes (Table 1) based on z_o from both methods. Mean gust factors for each of the four regimes differed by less than 2% using ratios of 2.60, 2.70, and 2.80. It is noted that the gust factor standard deviations were always larger for eddy-covariance-based z_o classes than for the TI method using the three values. The difference decreased from a maximum of 10% for smooth exposure to 4% for rough exposure observations with little variation resulting from the three values. When comparing the two gust factor distributions (TI method z_o and eddy-covariance z_o) for the roughness classes using a two-sample Kolmogorov–Smirnov (KS) test, the null hypothesis was rejected at the 90% confidence interval for all. This result highlights the difficulty in assessing the true surface roughness length and the relative uncertainty when mean wind speeds are standardized for height and/or exposure. The eddy-covariance method resulted in a larger envelope of gust factors included in each class, with the largest differences in the smooth and open regimes for this subset of data.

A qualitative roughness assessment through aerial photography was explored but has been shown to produce large errors. It led to a bias toward rougher terrain and the errors were considered too large for use here (Wieringa 1992; Powell et al. 1996; Schroeder et al. 2009). The profile method for WEMITE and FCMP towers was also considered, as these platforms employ multiple levels of anemometry. It was noted by Schroeder et al. (2009) that this method produced erroneous estimates from transitional flow regimes. Given the very large percentage of nonmarine wind observations within the dataset, it is difficult to determine which wind records were not influenced by transitional flow. The method also is not applicable to PMT or StickNet platforms.

The TI method was considered acceptable for the objective roughness classification applying a constant ratio of $\sigma_u/u_* = 2.70$. The analysis method used here allowed for z_o to vary temporally with changes in wind speed but not upstream fetch. It is possible that large turbulence intensities will result in an increase in the calculated z_o and that a convectively induced gust will be placed in a larger roughness category. It is also accepted that some differences in gust factor distributions between exposure classes will arise as a result of this method, and influences from dynamical processes could remain hidden within the variability.

Another concern is that both the TI and eddy-covariance methods assume neutral static stability in the HBL. Quantifying static stability over the depth of

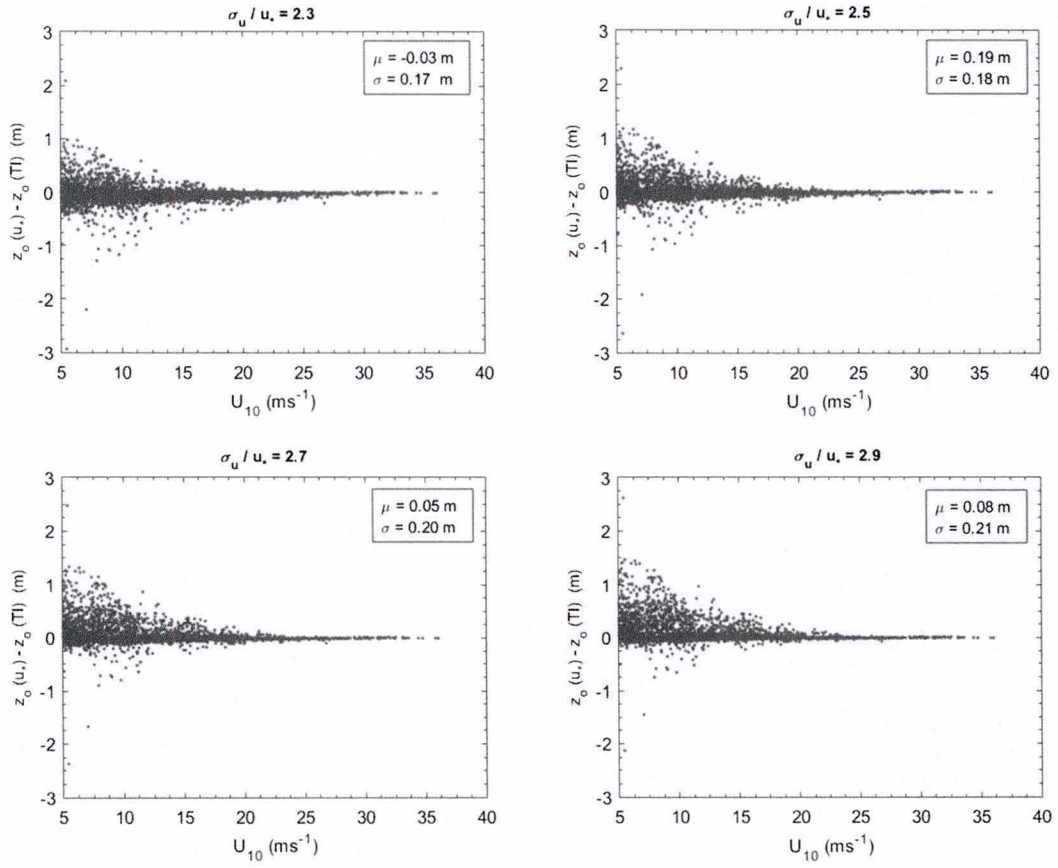

FIG. 1. TI method z_o values subtracted from the eddy-covariance z_o values shown as a function of the 10-min mean wind speed for selected constants of σ_u/u_*. The data shown here are from FCMP tower observations, which allows for both roughness-assessment methods to be used.

the HBL (including the surface layer) on land is very difficult. There remain very few high-resolution in situ thermodynamic vertical profile measurements within the HBL over land to help validate this assumption. Zhang et al. (2009) examined overwater turbulent fluxes calculated from turbulence probe observations in regions between rainbands (Black et al. 2007). Momentum flux profiles indicated a boundary layer depth nearly twice that indicated by GPS dropwindsonde (GPS sonde) thermodynamic profiles. Zhang et al. (2011) aggregated the thermodynamic data from a large number of GPS sondes over water into mean profiles and found a nearly constant layer of virtual potential temperature from the surface to 200 m. Composite Richardson number analysis based on the mean profiles also supported a general neutral or weakly stratified HBL (Zhang et al. 2011).

Beginning with Barnes et al. (1983) and Powell (1990), it has been shown in historical literature that convective-scale downdrafts can modify boundary layer air through deficits in potential temperature θ, equivalent potential temperature θ_e, and virtual potential temperature θ_v, especially within rainband convection (Barnes et al. 1983; Barnes and Stossmeister 1986; Powell 1990; Cione et al. 2000; Skwira et al. 2005; Knupp et al. 2006; Eastin et al. 2012; Molinari et al. 2013). Molinari et al. (2013) and Eastin et al. (2012) identified surface thermodynamic deficits over water and at landfall, respectively. It was shown that the source region of the identified cold pools may reside near 1-km height, but it remains unclear if the thermodynamic deficits meaningfully influence the local wind flow characteristics. The spatial resolution offered by TTU's StickNet observing network could help identify any effects.

3. Mean wind speed influences

The stratification of observations into their respective roughness categories allowed for secondary dependencies to be evaluated. Within neutrally stratified boundary layers, the influence of mean wind speed upon the turbulent wind flow characteristics is expected to be

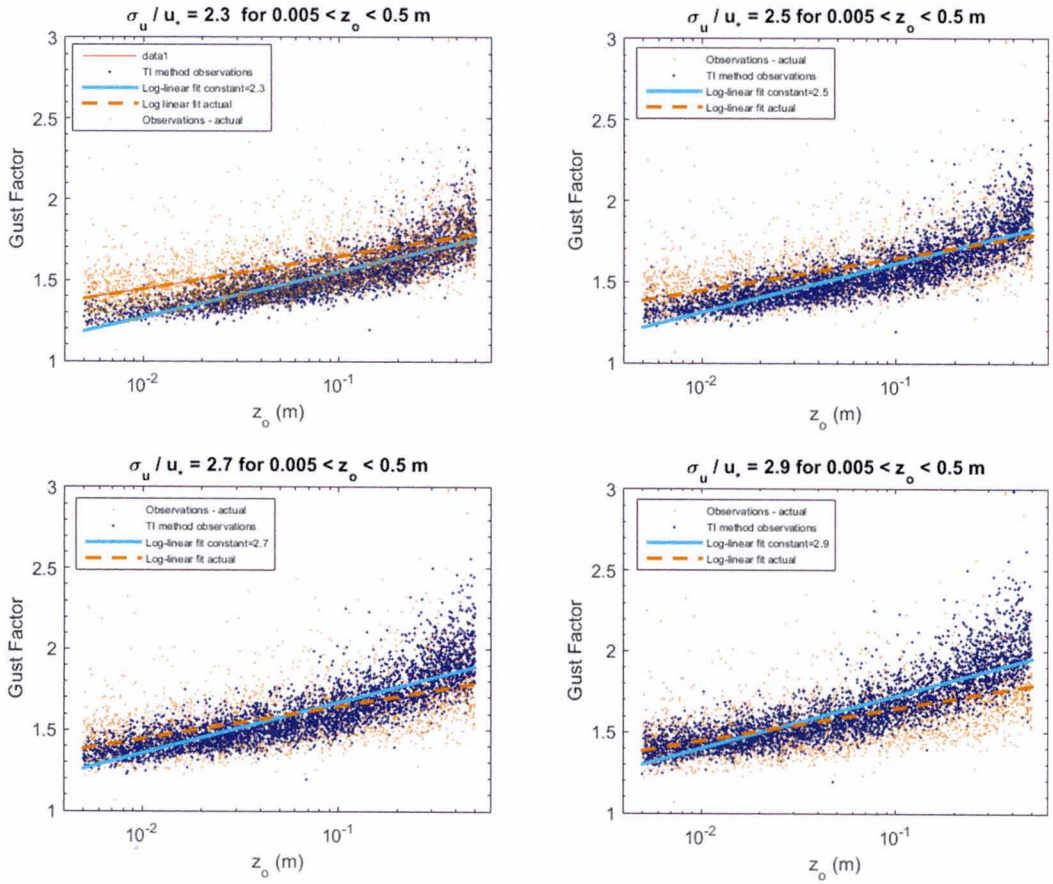

FIG. 2. Gust factors and their associated roughness lengths for FCMP observations computed using the eddy-covariance method (orange) and those found using the turbulence intensity method (blue) for selected σ_u/u_* constants. Log-linear fits are also provided. It should be noted that not all ratios used in the sensitivity analysis are shown.

minimal given that all other conditions remain constant. The peak winds within the dataset were found in smooth terrain exposure and the largest gust factors found within the rough exposure category. The peak 10-min mean wind speed within the complete dataset was $37\,m\,s^{-1}$, observed during Hurricane Rita (2005) in smooth terrain exposure (WEMITE 2 and FCMP T0, collocated). Gust factors were examined as a function of their associated 10-min mean wind speed and were grouped using $5\,m\,s^{-1}$ bin sizes by the following: 0–4.99, 5–9.99, 10–14.99, 15–19.99, 20–24.99, 25–29.99, 30–34.99, and $>35.00\,m\,s^{-1}$.

Gust factors within the smooth and open exposure regimes at 10 m contained little no meaningful trend with mean wind speed and did not exceed 2.00 within the smooth and open classes (Fig. 3). The gust factor distributions for each mean wind group within the two exposure classes were compared using a two-sample KS test. In the smooth exposure class, for mean wind groups below $20\,m\,s^{-1}$ the gust factor distributions were found to come from the same parent distribution. For open exposure observations, the underlying gust factor distributions for all mean wind groups were found to be from the same parent distribution. At higher mean winds, there was some evidence of a slight decrease in mean gust factors. The roughly open and rough exposure classes exhibited a reduction in gust factors with increasing mean winds of 5% and 10%, respectively (Fig. 3). It was noted that 10-m mean wind speeds did not exceed $30\,m\,s^{-1}$ within the roughly open classification and did not exceed $13\,m\,s^{-1}$ for the rough terrain exposure class.

The 2.25-m observations showed a trend toward decreasing mean gust factors with increasing mean winds in the smooth, open, and roughly open classes (note the small sample size in the rough terrain classification). Statistical distribution testing rejected the null hypothesis in all comparisons for 2.25-m observations. The large sample sizes from TTU StickNet observations in smoother exposure regimes may help in determining if a

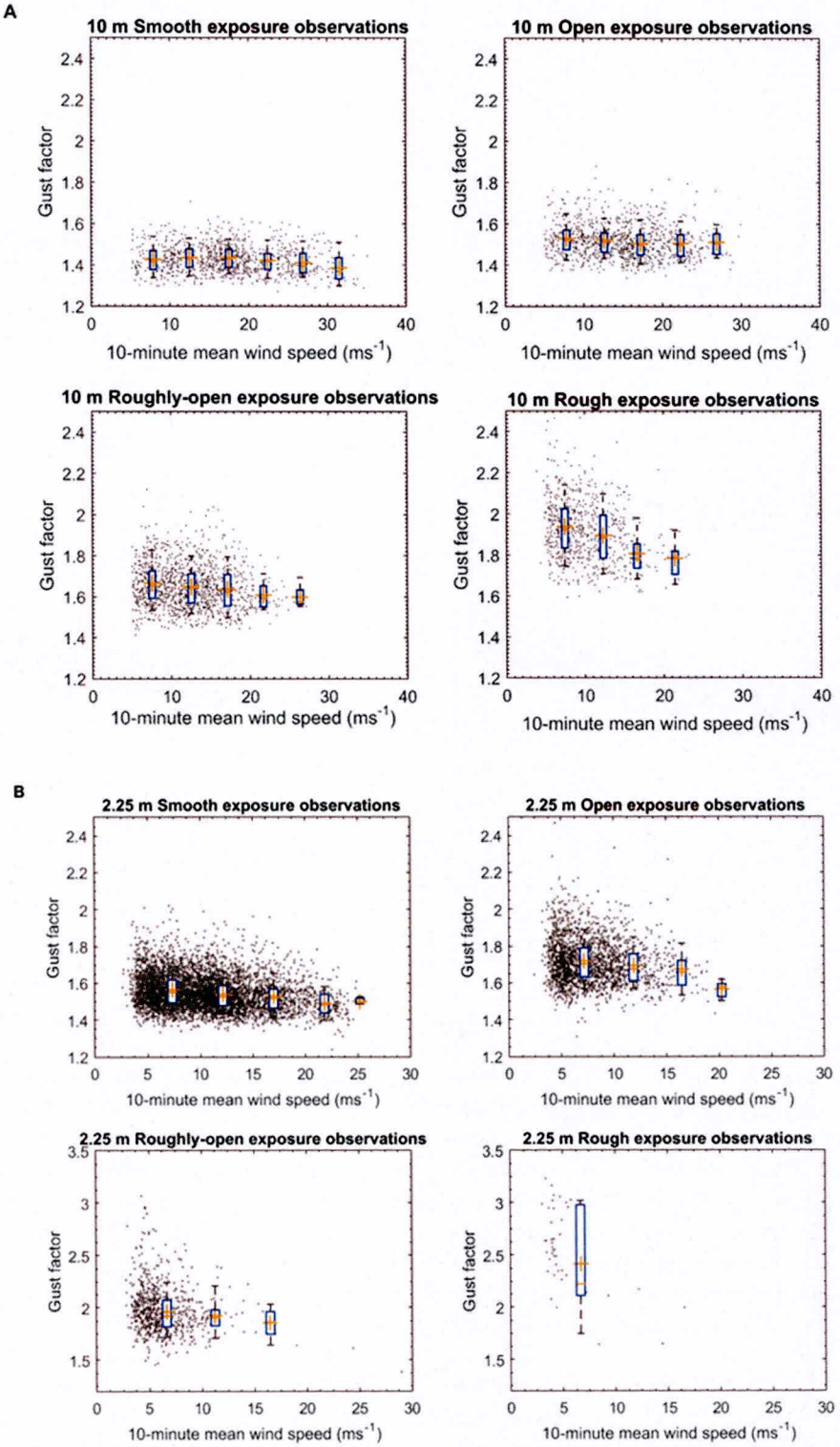

FIG. 3. Gust factors shown as a function of 10-min mean wind speed for (a) 10-m observations and (b) 2.25-m observations. Box-and-whisker plots represent gust factors grouped by mean wind speed. The mean and median are indicated. The box size represents the 25th and 75th percentiles, and the whiskers represent the 10th and 90th percentiles of the distribution for each group.

true relationship is present. An additional cause may be the deformation of surrounding vegetation as mean winds increase, as mentioned by Mahrt et al. (2001). The result would be a reduction in the height of local upstream roughness elements and lower gust factors. One would expect this effect to be more evident within the observations at 2.25 m. In addition, freshwater and storm surge inundation near observing platforms has been postulated to reduce z_o values with no change in wind direction (Edwards et al. 2014). This occurred at a few StickNet probes during Hurricanes Dolly (2008) and Ike (2008) but the sample in these conditions is small relative to the overall size of the StickNet portion of the dataset.

At 2.25 m, three gust factors greater than 2.00 were found in the smooth exposure class. In the other exposures classes, 198 observations exceeded 2.00. Of these, only 21 occurred in mean winds above $10\,m\,s^{-1}$ and 3 occurred in mean winds greater than $16\,m\,s^{-1}$. The mean gust factors for 2.25-m observations exhibited a decrease of 11% within the smooth exposure class between 10 and $30\,m\,s^{-1}$. It is noted that the sample size of the 30–$34.99\,m\,s^{-1}$ group at 2.25 m was composed of only three observations. The range of gust factors was also somewhat dependent upon mean wind with an observed decrease in the gust envelope with increasing speed. The 2.25-m observations, as expected, exhibited a larger difference in mean gust factors between the roughness classes at low wind speeds. However, as mean winds increased above $15\,m\,s^{-1}$, mean factors fell between 1.35 and 1.75.

4. Influence of storm-relative position

Observations and computational studies have shown that the structure of the HBL can change with azimuth and radius from the storm center (Kepert 2001; Kepert and Wang 2001; Kepert 2006a,b; Schwendike and Kepert 2008; Zhang et al. 2011; Giammanco et al. 2013). The depth of the boundary layer and the associated wind speed maximum was found to decrease toward the center (Kepert 2006a,b; Zhang et al. 2011; Giammanco et al. 2013). It was also suggested by Powell et al. (2003) that the wind maximum aloft could be considered as a reasonable upper bound for expected near-surface wind gusts. This rule of thumb is often used as qualitative guidance for operational meteorologists. Zhang et al. (2011) and Giammanco et al. (2013) showed that the general structure of the wind maximum aloft followed a similar trend with radius as that shown in the near-surface wind flow characteristics by Schroeder et al. (2009). The correlation with observed vertical wind profile changes was more pronounced in the results of Schroeder et al. (2009) than that shown here.

The slight reduction in gust factors with increasing mean wind speed indicated a weak radial dependence as the eyewall region near the radius of maximum winds (RMW) will contain the highest wind speeds; it also contains the lowest altitude of the wind speed maximum even at landfall (Kepert 2001; Franklin et al. 2003; Kepert 2006a,b; Zhang et al. 2011; Giammanco et al. 2013). Observations for each measuring height and roughness classification were stratified by radial distance from the tropical cyclone center. To view the wind observations from a storm-relative perspective, a high-resolution track was generated for each event over the duration of observations. Available center fixes based on flight-level data using the Willoughby and Chelmow (1982) algorithm were coupled with best-track center locations. These data are contained within the NOAA Hurricane Research Division H*Wind database and were subjectively quality controlled to remove discontinuities between the various center fixes. A smoothing spline was then fitted to the latitude and longitude time histories to produce a fitted track such that the radial distance and azimuth angle to the center of the hurricane could be calculated for each data segment. It was used effectively for assigning radii to Doppler radar–derived wind profiles by Giammanco et al. (2013) and Krupar (2015). In addition, radial distance was scaled by an estimate of the surface RMW. H*Wind surface wind field analyses were used to estimate the surface RMW for each tropical cyclone at landfall (Powell et al. 1998). The wind field was subdivided into four quadrants aligned with the direction of motion. A least squares polynomial best-fit was used to interpolate between H*Wind analyses. This produced a continuous time history of the evolution of the surface RMW in each quadrant over the temporal domain of an individual wind record (Giammanco et al. 2013). The associated surface RMW was assigned to the 10-min data segment for the quadrant in which the observing platform was located. Postevent wind field analyses were used when available. H*Wind analyses typically included the tower observations used in this study (Powell et al. 2010). It is noted that rapid structural changes can lead to large errors in estimating the true evolution of the surface RMW based on the relatively coarse wind field analysis time steps (typically 3 h).

Observations were binned using the following radial groups: <40, 40–80, 80–150, 150–250, and >250 km, which were dictated by the radial distribution of the observations. In general, gust factors increased slightly with radial distance (Fig. 4). At both measurement heights in most roughness classes, the linear trend had a positive slope. The exception was for 10-m observations in smooth terrain, which remained between 1.35 and

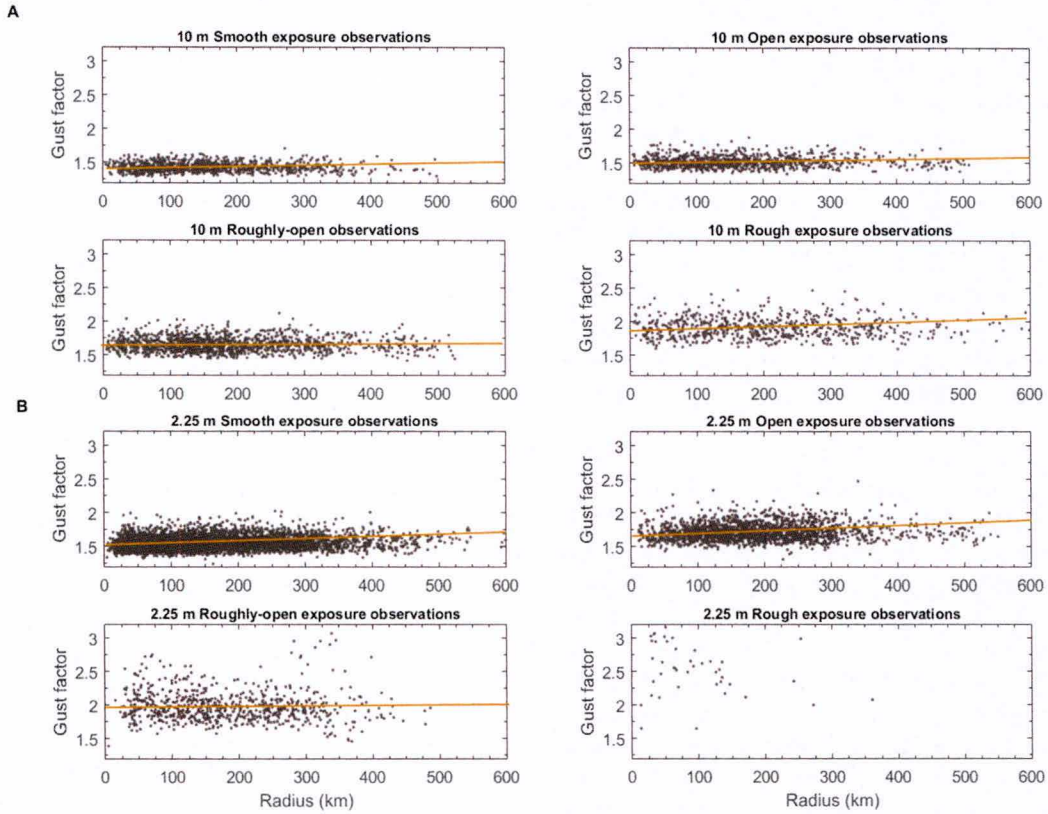

FIG. 4. Gust factors shown as a function of radial distance for (a) 10-m observations and (b) 2.25-m observations. The linear trend line for each exposure category is shown except for 2.25-m rough exposure, which had a very small sample size relative to the other 2.25-m observation groups.

1.45 for the five radial groups. The sample size for rough terrain observations at 2.25 m was too small for meaningful analysis.

Gust factors were also binned by their associated scaled radius using the following groups: <1, 1–1.5, 1.5–3, 3–5, and >5, which were based upon the quartiles of the distribution for the complete dataset. Within a storm-relative framework (Fig. 5), only the smooth regime contained an identifiable trend of increasing gust factors with increasing scaled radii. For the other exposure classes, mean gust factors at 10 m showed some variability but no meaningful trend. There was a slight reduction in gust factors at 10 m moving inward across the RMW, which is likely intertwined with the mean wind trend noted previously as winds decrease radially inward from the surface RMW. At 2.25 m for the smooth and open exposure classes, gust factors increased slightly with increasing scaled radii. Storm-relative influences such as tropical cyclone size, through the characteristics of the wind maximum aloft, would be masked within this framework. The minor trends noted with mean wind speed and unscaled radial distance indicate that some secondary influences to peak gust factors may be contained in the distribution, but any perturbations beyond what would be anticipated based on upstream terrain appear small.

5. Precipitation structure

The influence of convective-scale features on the near-surface gust characteristics has been mentioned within historical literature, with Fujita (1985, 1992) postulating that convective downbursts could produce "extreme" near-surface wind gusts and subkilometer damage gradients. Observational studies have found these to be rare and very difficult to observe in landfalling hurricanes (Bradbury et al. 1994; Sparks and Huang 2001; Schroeder and Smith 2003; Paulsen and Schroeder 2005; Vickery and Skerlj 2005; Schroeder et al. 2009). Composite radar reflectivity data from coastal WSR-88D were merged with the near-surface observations to investigate the influence of precipitation structure and eyewall passages on the wind flow characteristics. The radar volume occurring within the temporal domain of the segment was used to characterize the precipitation structure. Data segments were assigned a

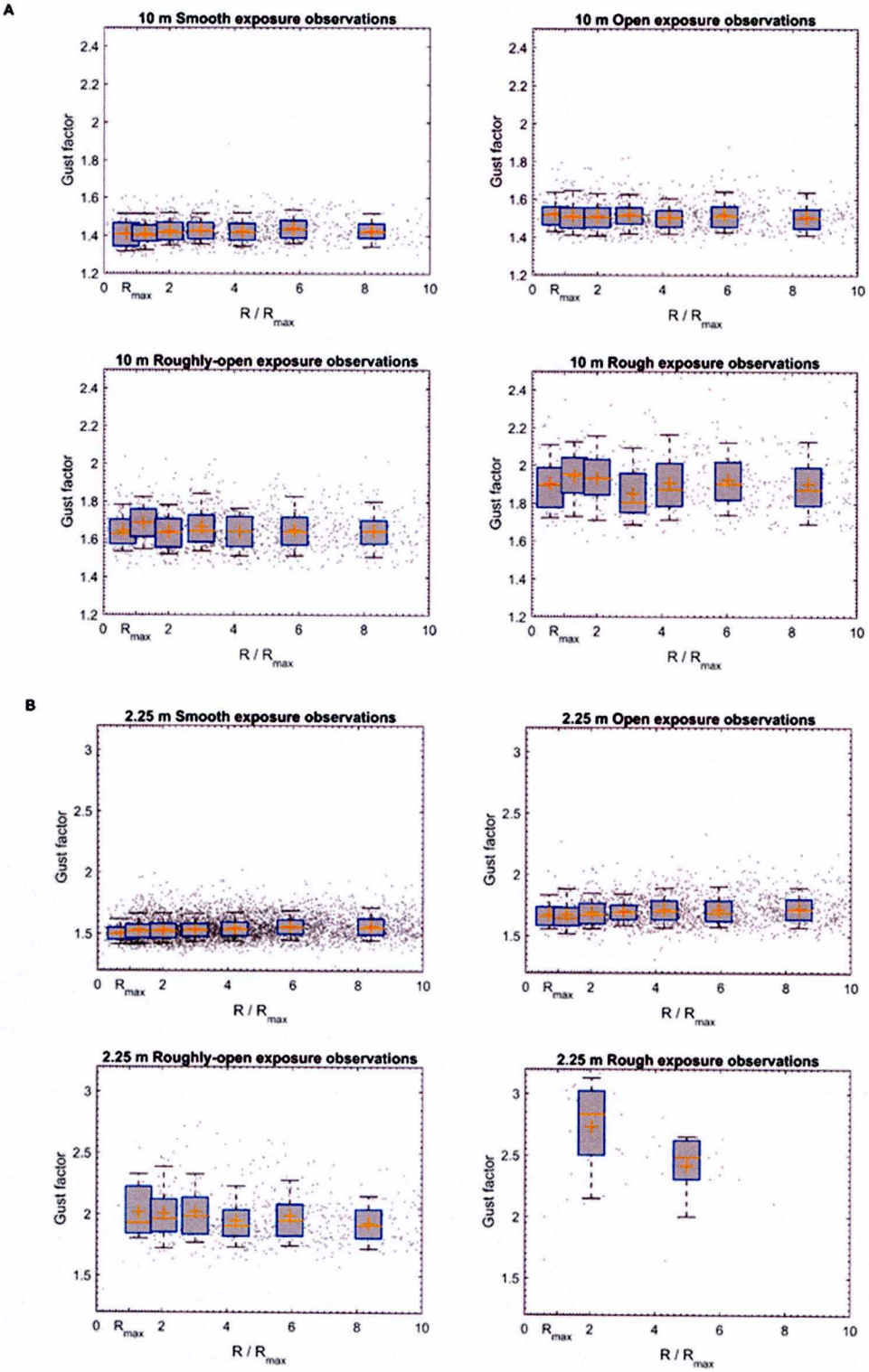

FIG. 5. Gust factors shown as a function of radial distance and distributions grouped by radial distance normalized by the surface RMW for (a) 10-m observations and (b) 2.25-m observations. For the box-and-whisker plots, the mean and median are indicated for each group. The box size represents the 25th and 75th percentiles, and the whiskers represent the 10th and 90th percentiles of the distribution for each group.

TABLE 3. Gust factor statistics for 10-m observations (WEMITE, FCMP) for smooth, open, roughly open, and rough exposures stratified by precipitation structure (convective–stratiform) and eyewall or outer vortex.

Statistic	Eyewall	Outer vortex: Stratiform	Outer vortex: Convective
Smooth			
Mean	1.46	1.43	1.43
Max	1.61	1.62	1.71
Min	1.31	1.27	1.29
Std dev	0.08	0.07	0.07
Mean wind speed	24.5	18.3	19.5
Sample size	20	465	164
Open			
Mean	1.51	1.52	1.52
Max	1.65	1.82	1.89
Min	1.41	1.35	1.38
Std dev	0.07	0.08	0.08
Mean wind speed	23.5	14.9	15.6
Sample size	39	438	201
Roughly open			
Mean	1.64	1.65	1.65
Max	1.89	2.03	2.12
Min	1.48	1.44	1.46
Std dev	0.06	0.11	0.14
Mean wind speed	21.5	14.1	15.2
Sample size	16	192	98
Rough			
Mean	1.81	1.89	1.94
Max	1.93	2.45	2.47
Min	1.64	1.59	1.62
Std dev	0.19	0.15	0.16
Mean wind speed	16.7	9.4	11.7
Sample size	14	269	142

qualitative assessment of the precipitation structure (e.g., convective or stratiform). Composite radar reflectivity data were interrogated to locate large horizontal gradients and to identify the melting level (i.e., bright band) using a vertical cross section. These features are indicative of convective or stratiform precipitation, respectively (Houze 1997). If no determination could be made, the observation was not assigned to a group. The methodology follows that of Schroeder et al. (2009). The use of an objective classification scheme such as that described by Churchill and Houze (1984) and used by Yuter and Houze (1995) and Didlake and Houze (2009) was investigated. The objective method showed little difference in identifying the two regimes when compared with a manual, subjective determination. A similar result was mentioned by Didlake and Houze (2009), who tuned their objective algorithms to match a similar method. In agreement with historical literature, the occurrence of observations made within stratiform precipitation regimes were approximately double those made within convective regimes (Jorgensen 1984; Marks 1985; Marks et al. 1992). Observations were also given a subjective outer-vortex or eyewall classification, similar to that used by Franklin et al. (2003) to classify GPS sonde profiles.

There was little change in 10-m mean gust factors with respect to region and precipitation structure. Only in rough terrain exposure did eyewall observations show a significant reduction (approximately 10%) between outer-vortex convective and stratiform observations. The range of gust factors was narrower for eyewall observations except in smooth exposure conditions. It is noted that for observations classified as "eyewall," gust factors did not exceed 2.00 at 10 m (Table 3). Within the open, roughly open, and rough terrain classifications, peak gust factors were largest for outer-vortex convective regimes, with a minimum for eyewall observations; mean gust factors showed little difference. The number of observations made within the eyewall was an order of magnitude less than those collected from outer-vortex convective and outer-vortex stratiform regions. Observations at 2.25 m were similar between the three regions but higher in value, which was to be expected for the lower measurement height (Table 4). It also indicated that convective features in outer rainbands contribute to larger peak gust factors and expanded ranges, but mean

TABLE 4. Gust factor statistics for 2.25-m observations (StickNet) for smooth, open, roughly open, and rough exposures stratified by precipitation structure (convective–stratiform) and eyewall or outer vortex.

Statistic	Eyewall	Outer vortex: Stratiform	Outer vortex: Convective
Smooth			
Mean	1.51	1.54	1.55
Max	1.69	1.99	2.02
Min	1.33	1.34	1.24
Std dev	0.08	0.09	0.10
Mean wind speed	19.3	12.0	12.5
Sample size	48	1668	1270
Open			
Mean	1.59	1.69	1.71
Max	1.78	2.16	2.27
Min	1.50	1.39	1.31
Std dev	0.09	0.12	0.12
Mean wind speed	17.5	9.3	9.2
Sample size	12	461	391
Roughly open			
Mean	—	1.89	1.98
Max	—	2.29	2.78
Min	—	1.57	1.47
Std dev	—	0.15	0.23
Mean wind speed	—	7.5	7.1
Sample size	1	85	171
Rough			
Mean	—	—	2.54
Max	—	—	3.07
Min	—	—	1.65
Std dev	—	—	0.40
Mean wind speed	—	—	5.3
Sample size	—	—	18

values exhibited only small differences. Although not presented, longitudinal integral length scales responded much more readily to the evolving precipitation structure at both measurement heights.

The vertical wind component w, when available, was averaged over the 3 s associated with the peak gust and normalized by the mean 10-min wind speed to examine the relationship between vertical motions and gust factors. As shown in Fig. 6, the surface roughness classification governed the distribution of gust factors. Vertical motions increased with rougher terrain exposures. Although larger vertical wind speeds generally were associated with relatively large gust factors, those greater than one standard deviation from the mean were also found at low vertical wind speeds ($|w| < 2\,\mathrm{m\,s^{-1}}$) within each roughness group. Normalized vertical winds in both precipitation regimes tended to support weak downward motion, with no evidence linking stronger near-surface downward motion to anomalously large gust factors outside of terrain effects. The influence of buoyancy-driven features, when compared with the underlying distribution within their respective roughness class, did not appear to depart from what was expected within their respective classes. Stratiform observations also exhibited larger variability across the range of normalized vertical velocities, but this may be due to the smaller sample of convective observations.

Composite reflectivity time histories for the radar volume over each platform's location were directly compared with near-surface observations to examine the influence of precipitation intensity and the near-surface wind field. Observations at 10 m revealed a slight increase in gust factors with increasing composite reflectivity within the open and roughly open classes; 2.25-m observations contained no trend (Fig. 7). When binned by composite reflectivity according to Schroeder et al. (2009), mean gust factors showed little dependence at the 10- and 2.25-m observation heights for all four exposure classifications (Fig. 7). Standard deviations did increase for observations within the rough exposure class with increasing composite reflectivity; however, the result may be due to the relatively small sample sizes within those reflectivity bins. The result differs from Schroeder et al. (2009), who found an increase in mean gust factors with increasing composite reflectivity. It is possible that the larger sample size and/or the longer data window (10 min) used here led to the difference. The data segments rejected for their lack of stationarity were typically

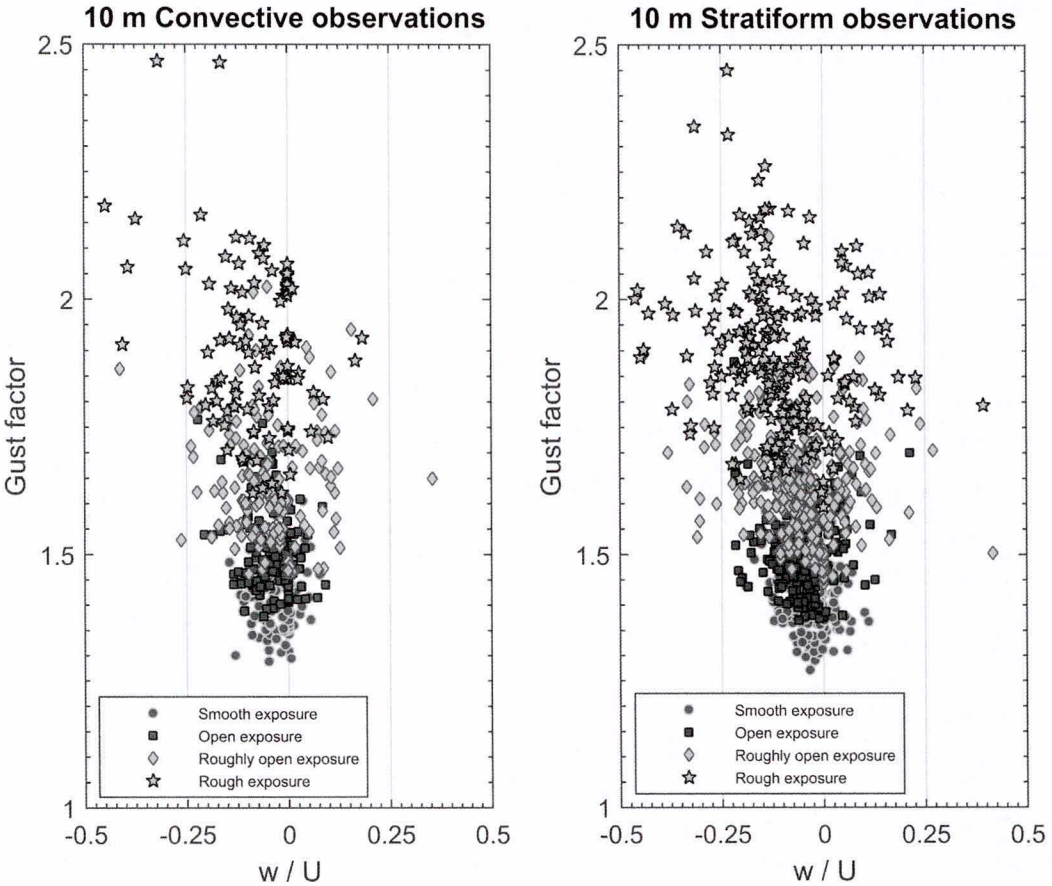

FIG. 6. Gust factors from identified (left) convective and (right) stratiform precipitation regimes shown as a function of their vertical wind component scaled by the 10-min mean wind speed U for each exposure classification.

found near rainband features in the outer-vortex region (approximately 75% of those segments rejected). The small changes between convective and stratiform regimes argue that the sole use of reflectivity information at volume coverage patterns (VCP) with long revisit times (>5 min) should not be used to infer near-surface gust characteristics. Recent improvements to WSR-88D VCP strategies, such as the Supplemental Adaptive Intra-Volume Low-Level Scan (SAILS) VCP, could help determine if a relationship is present and if operational guidance can be extracted. A dedicated field campaign using mobile research radars, deployable towers, and in situ disdrometers or particle imaging probes such as those discussed by Lopez et al. (2011) would be beneficial in understanding how precipitation processes in tropical cyclones affect the near-surface winds.

6. Storm-to-storm variability

Kepert (2001) and Kepert and Wang (2001) argue that the vertical structure of the HBL will vary from storm to storm and over the lifetime of a storm as its radial structure evolves. It has been shown that the size of the tropical cyclone determines both the height and relative magnitude of the wind speed maximum near the top of the boundary layer (Kepert 2006a,b; Schwendike and Kepert 2008). It is hypothesized that the shape of the vertical wind profile can influence the near-surface wind flow characteristics, with all other exposure conditions being equal.

Observations were segregated by both roughness classification and individual tropical cyclone. The summary statistics provided in Table 5 showed small differences in the mean gust factor from storm to storm within the same exposure class. Segregating by individual events limited the sample size within each classification. This was especially true for WEMITE and FCMP 10-m observations. The larger number of samples available for 2.25-m observations within a single event minimized the issue. As expected, the mean gust factors at 2.25 m were typically 10%–20% larger than those at 10 m except in the rough exposure class. Among

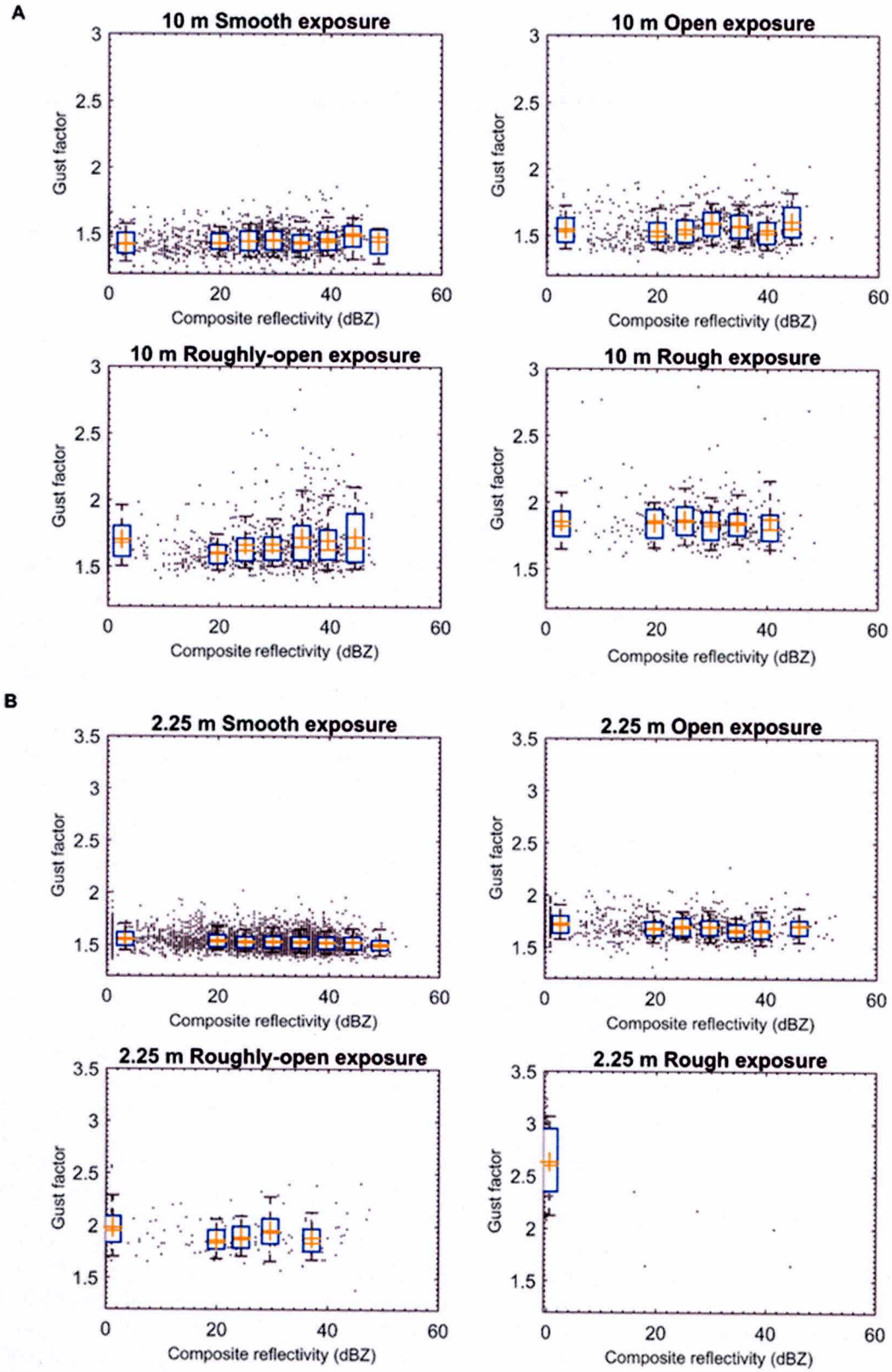

FIG. 7. Gust factors for (a) 10-m observations and (b) 2.25-m observations shown as a function of composite reflectivity and for observations grouped by composite reflectivity for each exposure class. For the box-and-whisker plots, the median and mean are indicated. The box size represents the 25th and 75th percentiles, and the whiskers represent the 10th and 90th percentiles of the distribution for each group.

TABLE 5. Gust factor statistics segregated by storm for smooth, open, roughly open, and rough terrain exposure classification. The mean wind speed for each group is also provided.

Storm	Smooth: Mean gust factor/mean wind speed	Open: Mean gust factor/mean wind speed	Roughly open: Mean gust factor/mean wind speed	Rough: Mean gust factor/mean wind speed
Charley (2004)	1.41/13.3	1.50/12.2	1.63/10.0	—
Ivan (2004)	1.43/20.5	1.52/14.5	1.64/12.3	1.95/9.2
Dennis (2005)	1.44/14.5	1.51/14.7	1.67/9.4	1.90/8.1
Katrina (2005)	1.44/16.8	1.53/14.5	1.68/12.3	1.91/9.7
Rita (2005)	1.45/15.7	1.51/14.8	1.64/12.3	1.79/14.6
Dolly (2008)[a]	1.54/9.6	1.69/6.8	1.99/6.5	—
Gustav (2008)	1.43/13.2	1.52/14.3	1.66/11.3	1.91/10.4
Gustav (2008)[a]	1.57/9.5	1.74/7.3	2.00/6.5	2.63/5.0
Ike (2008)	1.40/19.0	1.51/15.7	1.64/13.7	1.93/10.0
Ike (2008)[a]	1.55/12.8	1.71/9.7	1.92/7.1	—

[a] Indicates 2.25-m observations.

observations at a common measurement height, mean gust factors deviated from storm to storm by a maximum of only 4%.

a. *Gust factor and z_o relationships*

The gust factors from each landfall event were examined as a function of their associated z_o and common measurement height (Fig. 8). The log-linear trend lines showed some differences between the different tropical cyclones. The result appeared to be due to sample size differences across the range of z_o values, especially at higher gust factors in rougher terrain. There was some evidence that the change in gust factors at 10 m with increasing z_o from Hurricanes Charley (2004), Ivan (2004), Dennis (2005), and Gustav (2008) departed from the overall slope. For 2.25-m observations, which contain some pure marine exposures, gust factors were nearly constant for small z_o values (<0.01 m), shown in Fig. 9. The general slope and shape to the overall gust factor with respect to the z_o relationship was similar to that observed at 10 m.

The relationship to mean wind speeds was examined (not shown) and observations at 10 m followed the weak trend of decreasing gust factors with mean wind speed outside of smooth terrain exposures. Values appeared to be purely governed by surface roughness characteristics. However, data collected from Hurricane Ivan (2004), Hurricane Dennis (2005), and Hurricane Gustav (2008) showed a more pronounced reduction in gust factors as mean winds increased, especially for roughness lengths greater than 0.03 m. At 2.25 m, gust factors tended to converge as mean wind speed increased within most roughness regimes. It is noted that StickNet probes were typically deployed in open or smoother terrain exposures, and thus data are lacking from rough exposures. Interestingly, Hurricane Dolly (2008) produced a large envelope of gust factors at low mean winds even within smoother terrain exposures. This was not observed in wind data captured during Hurricane Ike (2008). In all three hurricanes, in which StickNet probes were deployed, 2.25-m gust factors converged to values between 1.30 and 1.40 for mean winds greater than 20 m s^{-1}. The higher number of StickNet probes and larger sample from an individual tropical cyclone are well suited for continuing this area of research as more datasets are collected. Fortunately for residents of the coastal United States, the few hurricane landfalls post-2008 limited this portion of the dataset.

b. *Influence of storm-relative position*

Observations in a storm-relative framework were used to examine the radial dependence of gust factors within individual storms. Although the general trend of a slight increase in gust factors with radial distance was present for observations at 10 m, two significant exceptions occurred. Gust factors in smooth terrain from Hurricanes Dennis (2005) and Gustav (2008) both decreased with radial distance, while those found in rougher conditions followed the expected trend. However, the envelope of observed gust factors from Hurricane Gustav (2008) was larger than that found during Hurricane Dennis (2005), with larger values found at large radii. This result may be due to the size of Hurricane Gustav (2008) (surface RMW of approximately 90 km at landfall) as compared with the relative compact structure of Hurricane Dennis (2005) (surface RMW of approximately 10 km at landfall) and its influence on the vertical wind profile. Hurricanes Ivan (2004), Katrina (2005), and Rita (2005) behaved similarly with regard to the radial distribution of gust factors, with only slight increases with radius. There were differences in the envelope of gust factor values from

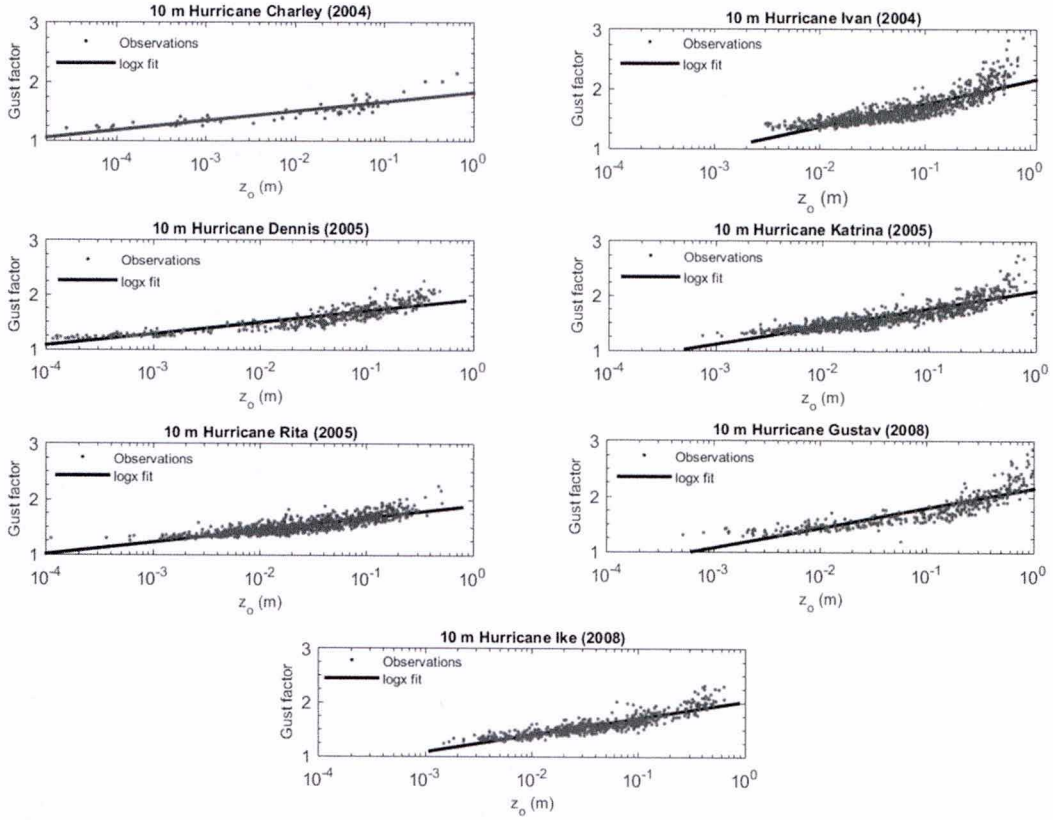

FIG. 8. Gust factors shown as a function of calculated z_o (using TI method with $\sigma_u/u_* = 2.70$) for 10-m observations from the landfalling tropical cyclones contained in this study.

storm to storm especially at radii greater than 100 km. Upon removing the influence of storm size by scaling radial distance by the RMW, the gust factor relationship did not deviate significantly. Of note was a slight increase in gust factor values across the RMW during Hurricane Katrina (2005) in smooth terrain.

Tropical cyclone observations stratified by eyewall or outer-vortex classification, terrain exposure, and precipitation structure were examined with respect to their parent storm. As shown in Tables 6 and 7, small differences from storm to storm were observed within the same classification of roughness and storm-relative position for observations made at 10 m. Eyewall mean gust factors were typically lower within their respective terrain exposure class and between the three regimes, but differences did not exceed 10%. The exception was Hurricane Ivan (2004) within the smooth, open, and rough terrain classes. Hurricane Rita (2005) at rough exposures produced relatively low gust factors by nearly 10% when compared with the other tropical cyclones with observations in this terrain category. Hurricanes Charley (2004) and Dennis (2005) had the lowest mean gust factors within all precipitation regimes, while Hurricane Ivan exhibited slightly higher values.

7. Comparisons of near-surface winds and gust factors with the vertical wind profile

a. KLIX and PMT-Clear observations of Hurricane Katrina (2005)

A unique comparison was possible utilizing the TTU PMT-Clear tower located at the Slidell (Louisiana) Municipal Airport during the landfall of Hurricane Katrina (2005). The tower was located very near (<2 km) the KLIX WSR-88D. The radial profile of velocity–azimuth display (VAD) HBL wind profiles, presented in Giammanco et al. (2013) and Krupar (2015), was examined along with the near-surface observations from the tower. The site experienced the passage of the northwestern eyewall, but the wind speed record did not have a defined local minimum, which indicated that the site did not enter the eye. For available profiles, the wind speed maximum aloft was compared with the time history of 3-s and 10-Hz gust wind speeds (Fig. 10). The difference between the

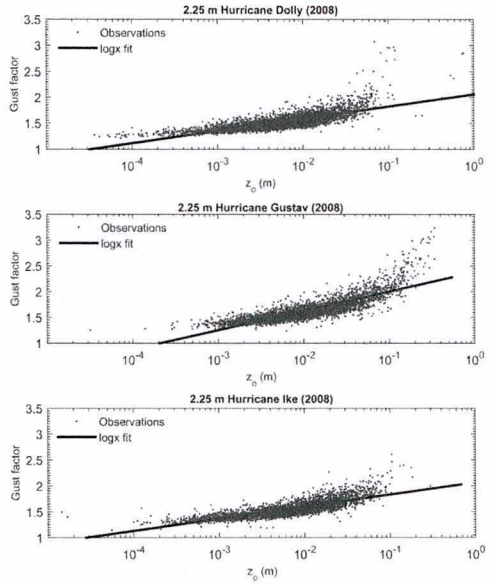

FIG. 9. As in Fig. 8, but for 2.25-m observations from the landfalling tropical cyclones sampled by TTU StickNet platforms.

peak near-surface gusts and the wind maximum aloft decreased from nearly 9 to 3 m s^{-1} as mean winds increased aloft and near the surface. During this time, the wind maximum descended from a mean height above the VAD vertical domain (1200 m) to near 500 m as the eyewall approached. The instantaneous (10 Hz) wind speed did not exceed the wind maximum aloft prior to the data transmission failure of the KLIX WSR-88D when the site was located approximately 100–110 km radially outward from the center.

The height at which the 10-Hz wind speed was within 0.5 m s^{-1} to the VAD-estimated wind was examined as an approximation of the effective mixing height. Within the vertical domain of VAD observations, the height at which the surface 10-Hz gust was equivalent to a VAD observation above remained near 350 m and did not change with radius (within 200 km of the center). The relatively consistent estimate of mixing depth was in agreement with the two primary fetches (northeasterly and southwesterly), which had similar z_o values between 0.10 and 0.20 m.

Two GPS sondes were launched within 30 km of the KLIX radar at 1116 and 1338 UTC. Each landed in Lake Pontchartrain to the south of KLIX and the PMT-Clear tower. Thermodynamic profiles (not shown) indicated a well-mixed layer extending to a height of 200–250 m, defined as the height where potential temperature θ fell below 0.5 K of its surface value. The kinematic data from the two profiles contained an absolute wind maximum near 1 km and a secondary maximum between 400 and −500 m, respectively. Several small-scale local wind maxima and minima were captured in the profiles (Franklin et al. 2003). The general structure is in agreement with the HBL height scales put forth by Zhang et al. (2011) with the typical differences between the kinematic and thermodynamic depths. Measured gusts did not reach the magnitude of the maximum aloft. In this case, the wind maximum appears to have resided above the thermodynamic mixed layer, which may not have allowed for the highest relative momentum associated with the low-level wind maximum to reach the surface.

b. KHGX and FCMP T4 and T1 observations of Hurricane Ike (2008)

A second case study was conducted to investigate the correlation between changes in the vertical wind profile and near-surface wind measurements. The landfall of Hurricane Ike (2008) offered a comparison between the FCMP T4 and T1 towers and the KHGX WSR-88D (Houston–Galveston, Texas). Although the towers were not collocated with the KHGX WSR-88D, the case offered a radial cross section of the northern and southern eyewalls of Hurricane Ike. The complete time histories from both towers exhibited a wind speed minimum of 2 m s^{-1}, while the VAD HBL time history from the lowest bin contained a minimum of 12 m s^{-1} as the center passed. It is noted that profiles from the inner edge of the eyewall into the eye may not meet the assumptions required by the VAD methodology, as a result of strong curvature of the flow and possible lack of scatterers. Despite these concerns, the technique still produced coherent wind speed estimates through the passage of the eye (Browning and Wexler 1968; Giammanco et al. 2013; Krupar 2015). It is also thought that the rapidly changing fetch and wind speed in this region could present a challenge in obtaining 10-min wind speed records that satisfy the stationarity criteria. However, most nonstationary segments were found during rainband passages with fewer than twenty 10-min segments rejected from eyewall samples across the three instrument platforms. Despite the large dataset assembled, the sample size of complete records through the eyewall into the eye was still relatively small.

The T4 tower was located approximately 20 km to the north-northeast of the KHGX radar site (outside the VAD domain) at the La Porte Municipal Airport (La Porte, Texas). The T1 tower was nearby in a suburban park approximately 1.7 km to the southwest of T4 located in a region of rough terrain exposure. It is noted that peak 10-Hz gusts from T1 did not exceed those observed by T4 or the VAD wind profile maxima. For the purpose of this case study, the T1 tower was ignored. The T4 tower, despite being located within an airfield,

TABLE 6. Mean gust factors and 10-min mean wind speed for 10-m observations (WEMITE, FCMP) stratified by storm, precipitation structure, and roughness classification.

Storm	Smooth gust factor/mean wind speed ($m\,s^{-1}$)	Open gust factor/mean wind speed ($m\,s^{-1}$)	Roughly open gust factor/mean wind speed ($m\,s^{-1}$)	Rough gust factor/mean wind speed ($m\,s^{-1}$)
Charley (2004)				
Eyewall	—	—	—	—
Outer vortex: Stratiform	—	1.50/14.8	1.65/9.9	—
Outer vortex: Convective	—	1.53/15.4	1.67/13.1	—
Ivan (2004)				
Eyewall	1.47/22.3	1.54/21.1	—	1.97/14.4
Outer vortex: Stratiform	1.43/21.8	1.52/13.8	1.64/12.0	1.90/8.5
Outer vortex: Convective	1.50/16.1	1.53/15.5	1.65/13.4	2.03/10.5
Dennis (2005)				
Eyewall	—	1.46/26.4	1.61/17.6	—
Outer vortex: Stratiform	1.43/11.2	1.51/15.2	1.66/9.8	1.90/8.0
Outer vortex: Convective	—	1.51/19.6	1.67/12.0	1.90/9.8
Katrina (2005)				
Eyewall	—	1.46/25.6	—	—
Outer vortex: Stratiform	1.45/16.6	1.52/14.6	1.67/10.8	1.94/8.6
Outer vortex: Convective	1.47/15.1	1.54/14.8	1.69/10.8	2.04/10.4
Rita (2005)				
Eyewall	—	1.49/23.4	1.64/23.1	1.78/21.2
Outer vortex: Stratiform	1.44/18.3	1.50/15.7	1.67/10.8	1.78/13.3
Outer vortex: Convective	1.44/17.5	1.52/18.3	1.69/10.8	1.81/16.4
Gustav (2008)				
Eyewall	—	—	—	—
Outer vortex: Stratiform	1.44/14.4	1.51/15.5	1.65/13.2	1.87/11.3
Outer vortex: Convective	1.44/17.5	1.55/14.1	1.66/13.5	1.92/14.2
Ike (2008)				
Eyewall	1.44/25.8	1.52/21.7	1.62/18.7	—
Outer vortex: Stratiform	1.40/19.8	1.52/15.0	1.61/13.4	1.84/10.2
Outer vortex: Convective	1.40/26.1	1.51/17.8	1.63/16.8	—

experienced roughness lengths near 0.10 m (roughly open) during the passage of RMW in the northern eyewall. Gust factors remained near 1.60 with little radial dependence observed within the record. Roughness length values increased slightly to 0.15 m with a transition to a general westerly fetch but remained within the roughly open classification. The peak gust factor within the complete record (1.77) occurred with the outer edge of the RMW just prior to the passage of the northern eyewall (Fig. 11).

During the passages of both the northern and southern eyewalls of Hurricane Ike (2008), the peak 10-Hz and peak 3-s gust wind speeds did not exceed the VAD wind speed maximum (Fig. 11). The radial profile of the VAD maximum was not very peaked and exhibited a broad decay with radial distance away from the storm center, likely resulting from the broad radial pressure gradient of Hurricane Ike (2008) (Berg 2009). The height of the wind maximum descended from approximately 900 m, near the top of the VAD domain, to a minimum altitude of 250 m radially inward from the RMW during the passage of the northern eyewall. The T4 observed gust wind speeds were 5–10 $m\,s^{-1}$ below the magnitude of the low-level wind maximum at radii greater than 60 km prior to the approach of the northern eyewall. A slight reduction was observed at 50-km radius, associated with a moat region and relative reflectivity minimum between the primary rainband and the approaching northern eyewall. It is unclear if changes in boundary layer stability may have suppressed vertical mixing within the moat and led to a temporary reduction in overall wind speeds (mean and gust). The wind maximum aloft sampled by the VAD HBL profiles did not show any evidence of this feature. The radius of maximum winds was sampled by both KHGX and T4 and peak 10-Hz gusts came within 1.5 $m\,s^{-1}$ of the wind maximum aloft as it descended from 800 to 360 m radially inward from the surface RMW.

The southern eyewall exhibited a lower wind maximum near 360 m that fluctuated between 250 and 360 m as radial distance increased as the storm moved northward away from KHGX. The observed T4 peak gust wind speeds remained nearly 15 $m\,s^{-1}$ below the observed VAD wind maximum as winds decreased. The

TABLE 7. Mean gust factors and 10-min mean wind speed for 2.25-m observations (StickNet) stratified by storm, precipitation structure, and roughness classification.

Storm	Smooth gust factor/mean wind speed ($m\,s^{-1}$)	Open gust factor/mean wind speed ($m\,s^{-1}$)	Roughly open gust factor/mean wind speed ($m\,s^{-1}$)	Rough gust factor/mean wind speed ($m\,s^{-1}$)
Dolly (2008)				
Eyewall	1.50/17.6	—	—	—
Outer vortex: Stratiform	1.53/10.6	1.67/7.7	1.81/7.1	—
Outer vortex: Convective	1.53/13.1	1.69/9.7	1.82/9.3	—
Gustav (2008)				
Eyewall	—	—	—	—
Outer vortex: Stratiform	1.54/18.6	1.72/13.9	2.00/6.2	—
Outer vortex: Convective	1.56/10.3	—	—	2.59/5.7
Ike (2008)				
Eyewall	1.52/20.4	1.61/17.1	—	—
Outer vortex: Stratiform	1.55/13.9	1.68/10.4	1.89/7.6	—
Outer vortex: Convective	1.55/15.9	1.71/12.7	1.97/10.9	—

decay in wind speed for both the VAD profile maximum and the tower winds were very similar as the storm center moved northward away from the sites.

8. Summary and discussion

The deployment of ruggedized observing systems by TTU and the FCMP provided a sizeable number of data records, the largest assembled to date, in which gust factors could be examined with respect to several factors. The records from FCMP platforms also allowed for a sensitivity comparison between z_o values using the TI method described by Beljaars (1987) and those determined using the classic eddy-covariance method. Classification of gust factors according to the TI method z_o is sensitive to the assumed value of the ratio of the standard deviation of the wind to the friction velocity. The historical literature assumes a value of 2.40 or 2.50; the results of Miller et al. (2015) and the analysis presented here indicate that a value between 2.70 and 2.90 is more appropriate for overland observations. The TI method roughness calculation, unlike other roughness-assessment methods (i.e., through aerial photography or the profile method), is a valuable tool to provide an objective assessment of terrain exposure when instrumentation characteristics and sampling do not allow for the eddy-covariance method to be applied. The sensitivity investigation of the TI method roughness length calculation helped shed light on the inherent uncertainties associated with the method that users should be aware of.

Observations were examined with respect to mean wind speed and radial and scaled radial distances. Data were also coupled with WSR-88D reflectivity records to study the influence of precipitation structure aloft on the local wind field. Two fortuitous comparison cases between VAD-derived vertical wind profiles and nearby observing platforms were made to examine how the near-surface wind flow may evolve with the wind speed maximum near or at the top of the boundary layer. The following summarizes the results and possible operational implications for understanding hurricane wind gust characteristics:

- Terrain exposure is the predominant driver of landfalling hurricane gust factors. Secondary influences appear small relative to those associated with upstream terrain changes.
- Gust factors decrease slightly with increasing mean winds near the radius of maximum winds. It is unlikely in open or smooth exposures for gust factors to routinely exceed 2.00.
- There is little difference between eyewall and outer-vortex convective or outer-vortex stratiform mean gust factors; however, outer-vortex convective regimes will exhibit a larger range of gust factors.
- Extreme gusts and the features capable of producing anomalous gust factors are rare and difficult to observe even when using improved spatial observation coverage.
- WSR-88D composite reflectivity showed little correlation with underlying near-surface gust factors. Its use to infer wind flow characteristics during landfalling hurricanes is discouraged. The use of mobile research radars may help define the true relationship between precipitation processes and near-surface wind flows.
- In two cases, near-surface wind gusts did not exceed the wind speed maximum near the top of the boundary layer. The use of the wind speed maximum aloft appears to be a reasonable rule of thumb to approximate the upper limit of instantaneous near-surface gusts. Peak 3-s gusts will be lower.

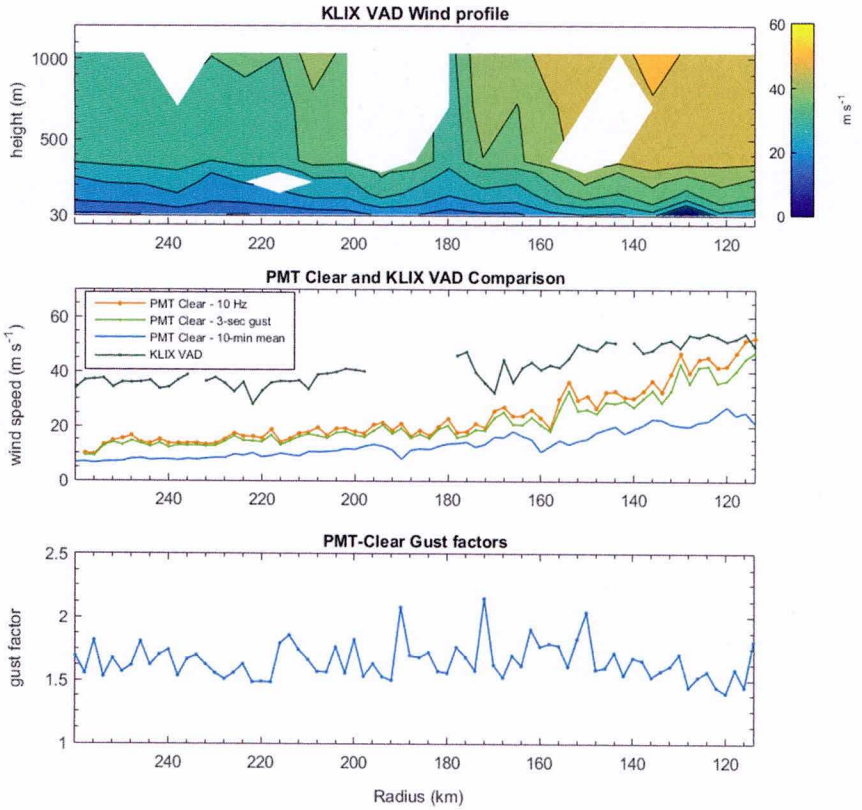

FIG. 10. Observations of the approach of the northern eyewall of Hurricane Katrina (2008) of (top) KLIX-derived VAD wind speed shown as a function of radius; (middle) PMT-Clear observed 10-min mean wind speed (blue), peak 3-s gust (light green), peak 10-Hz wind speed (orange), and the VAD-derived wind speed maximum (dark green); and (bottom) PMT-Clear gust factors shown as a function of radial distance.

The presence of coherent features in the HBL and tropical cyclone eyewall has been observed to modulate the near-surface wind field. The ability of transient mesoscale features to produce anomalous gusts has been observed, but several recent studies have shown them to be rare and difficult to observe. The recent results of Schroeder et al. (2009), Harper et al. (2010), and Miller et al. (2015) and those presented here indicate that wind gusts in the eyewall region are not appreciably different than other regions. Upstream fetch and small-scale terrain changes are the dominant controls on the turbulence quantities. Despite the large sample size relative to other historical studies, the overall sample of hurricane eyewall conditions is still quite small. Improving spatial coverage using a denser network of observing stations may eventually determine the near-surface characteristics associated with transient mesoscale features.

The small radial dependence noted in this study at rougher exposures was similar to the change in the relative magnitude of the wind speed maximum aloft found in composite vertical wind profiles (Zhang et al. 2011; Giammanco et al. 2013). This result may be tied to the reduction in mean wind due to the rougher exposure, while the wind maximum aloft (i.e., momentum source) does not appreciably respond to small-scale spatial changes in terrain. In smoother regimes, the flow approaches the gradient wind driven by the horizontal pressure gradient, reducing the difference between the wind speed maximum aloft. It is also hypothesized that given a decreasing scaled wind maximum aloft at small radial distances, the relative vertical momentum available for transport to the surface as a gust feature is reduced. These factors partially explain the lack of extreme gusts within the eyewall region. It is noted that Kepert (2006a,b) suggested that the character of the wind maximum aloft is likely influenced by storm size through the shape of the radial profile of the gradient wind. It is plausible that tropical cyclones with a peaked radial pressure profile and potentially a supergradient low-level wind maximum could produce higher gust factors across the terrain classes. Within the dataset used here, only Hurricanes Charley (2004) and Dennis (2005) approach the type of tropical cyclone described by Kepert (2001), Kepert and Wang (2001), and Kepert

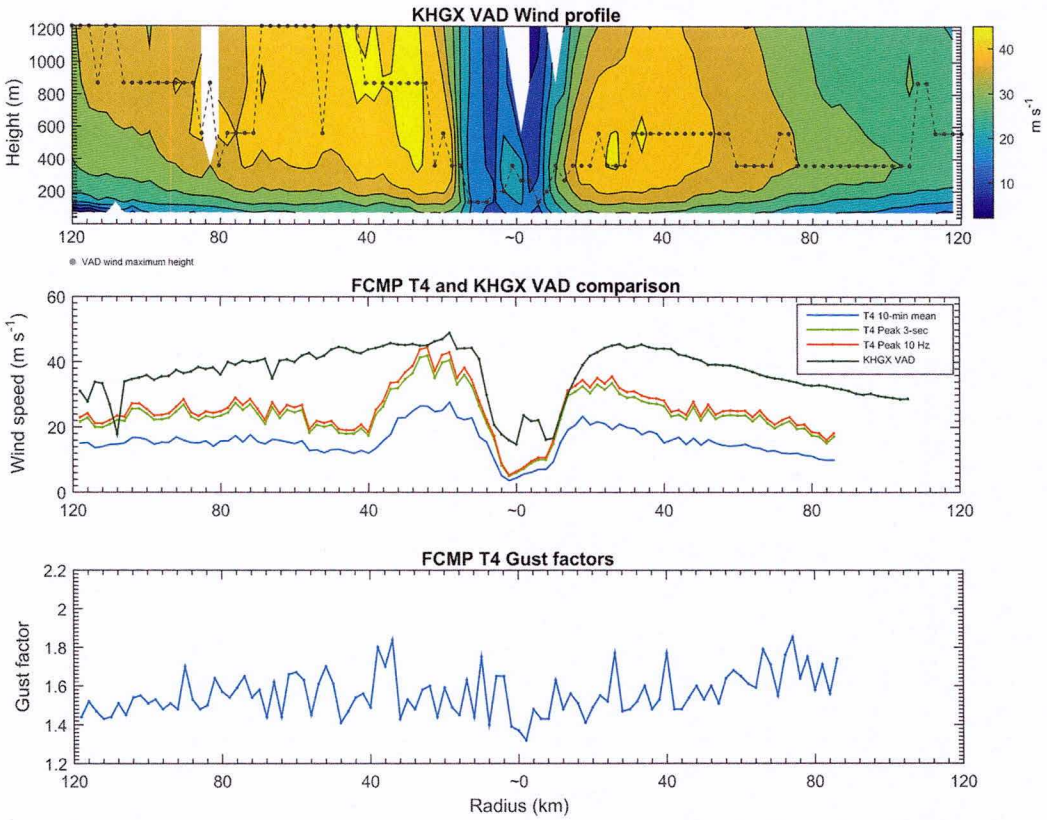

FIG. 11. Observations of the passage of the northern and southern eyewall of Hurricane Ike (2008) of (top) KHGX-derived VAD wind speed and the height of the profile wind speed maximum (dashed gray); (middle) T4 observed 10-min mean wind speed (blue), peak 3-s gust (light green), peak 10-Hz wind speed (orange), and the VAD-derived wind speed maximum (dark green); and (bottom) gust factors from the T4 tower shown as a function of radial distance.

(2006a,b) that would produce these characteristics. Unfortunately, the sample sizes from the two storms are small relative to others in the archive and lack a meaningful number of eyewall observations.

The difference between surface gust wind speeds and the wind maximum above decreased when the relationship between vertical wind profiles with respect to the near-surface wind flow was investigated. The general descent in the height of the wind maximum aloft toward the cyclone center and the possibility of deeper mixing within the eyewall may be contributing factors along with the radial pressure profile that are inherently linked through the mechanisms shown by Kepert (2001) and Kepert and Wang (2001). Diagnosis of the wind maximum aloft and its altitude through aircraft reconnaissance, GPS sondes, and VAD wind profiles could allow for improved operational expectations of the maximum possible gusts as a tropical cyclone makes landfall. This may improve wind gust estimates from numerical weather prediction model output that are capable of resolving the low-level wind maximum. The output could be coupled with underlying high-resolution land-use datasets to produce more accurate maximum wind gust forecasts for various exposures in a landfall region that account for storm-scale processes and their influences.

The near-surface observations presented here represent the largest archive of tropical cyclone wind measurements assembled to date. However, the data are primarily representative of overland exposures. Unfortunately, only a small fraction of the archive was collected in true marine exposure conditions and in 10-min mean wind speeds exceeding $35\,\mathrm{m\,s^{-1}}$. There remains a significant need to collect critical near-surface measurements in both overland and marine exposure conditions in higher mean wind speeds and within the tropical cyclone eyewall. Additional work is also needed to understand the relationship between the near-surface wind flow and associated vertical wind profiles.

Acknowledgments. The foundation for this work was first presented at the American Meteorological Society's 30th Conference on Hurricanes and Tropical Meteorology.

The authors sincerely thank the faculty, staff, and students that have participated in the safe deployment of research instrumentation by Texas Tech University and the institutions within the Florida Coastal Monitoring Program since 1998. Financial support for the data analysis was provided by Applied Research Associates and DeepStar. TTU data collection deployments were funded through a National Institute of Standards and Technology (NIST) Cooperative Agreement Award (70NANB8H0059) and the National Science Foundation (NSF) (ATM-0134188). FCMP data collection efforts were supported in part by NSF CMMI-0625124 and CMMI-0928563. The authors extend their thanks to the three anonymous reviewers whose commentary and suggestions improved the quality of this paper. The authors acknowledge Theresa Aguilar at Texas Tech University for assistance in compiling WEMITE 2.5-m wind records and Christine Alfano from the Insurance Institute for Business and Home Safety for a review of this paper.

REFERENCES

Ashcroft, J., 1994: The relationship between the gust ratio, terrain roughness, gust duration and the hourly mean wind speed. *J. Wind Eng. Ind. Aerodyn.*, **53**, 331–355, doi:10.1016/0167-6105(94)90090-6.

Balderrama, J.-A., and Coauthors, 2011: The Florida Coastal Monitoring Program (FCMP): A review. *J. Wind Eng. Ind. Aerodyn.*, **99**, 979–995, doi:10.1016/j.jweia.2011.07.002.

Barnes, G. M., and G. J. Stossmeister, 1986: The structure and decay of a rainband in Hurricane Irene (1981). *Mon. Wea. Rev.*, **114**, 2590–2601, doi:10.1175/1520-0493(1986)114<2590:TSADOA>2.0.CO;2.

——, E. J. Zipser, D. Jorgensen, and F. D. Marks, 1983: Mesoscale and convective structure of a hurricane rainband. *J. Atmos. Sci.*, **40**, 2125–2137, doi:10.1175/1520-0469(1983)040<2125:MACSOA>2.0.CO;2.

Beljaars, A. C. M., 1987: The measurement of gustiness at routine wind stations—A review. KNMI Rep. WR87-11, 50 pp. [Available online at http://bibliotheek.knmi.nl/knmipubWR/WR87-11.pdf.]

Berg, R., 2009: Tropical cyclone report: Hurricane Ike (AL092008) 1–14 September 2008. National Hurricane Center Rep., 55 pp. [Available online at http://www.nhc.noaa.gov/data/tcr/AL092008_Ike.pdf.]

Black, M. L., R. W. Burpee, and F. D. Marks, 1996: Vertical motion characteristics of tropical cyclones determined with airborne Doppler radial velocities. *J. Atmos. Sci.*, **53**, 1887–1909, doi:10.1175/1520-0469(1996)053<1887:VMCOTC>2.0.CO;2.

Black, P. G., and Coauthors, 2007: Air–sea exchange in hurricanes: Synthesis of observations from the Coupled Boundary Layer Air–Sea Transfer experiment. *Bull. Amer. Meteor. Soc.*, **88**, 357–374, doi:10.1175/BAMS-88-3-357.

Blessing, C., and F. J. Masters, 2005: Attrition of ground weather observations during hurricane landfall. *Proc. 10th Americas Conf. on Wind Engineering*, Baton Rouge, LA, American Association for Wind Engineering.

Bradbury, W. M. S., D. M. Deaves, J. C. R. Hunt, R. Kershaw, K. Nakamura, M. E. Hardman, and P. W. Bearman, 1994: The importance of convective gusts. *Meteor. Appl.*, **1**, 365–378, doi:10.1002/met.5060010407.

Browning, K. A., and R. Wexler, 1968: The determination of kinematic properties of a wind field using Doppler radar. *J. Appl. Meteor.*, **7**, 105–113, doi:10.1175/1520-0450(1968)007<0105:TDOKPO>2.0.CO;2.

Churchill, D. D., and R. A. Houze Jr., 1984: Development and structure of winter monsoon cloud clusters on 10 December 1978. *J. Atmos. Sci.*, **41**, 933–960, doi:10.1175/1520-0469(1984)041<0933:DASOWM>2.0.CO;2.

Cione, J. J., P. G. Black, and S. H. Houston, 2000: Surface observations in the hurricane environment. *Mon. Wea. Rev.*, **128**, 1550–1561, doi:10.1175/1520-0493(2000)128<1550:SOITHE>2.0.CO;2.

Didlake, A. C., Jr., and R. A. Houze Jr., 2009: Convective-scale downdrafts in the principal rainband of Hurricane Katrina (2005). *Mon. Wea. Rev.*, **137**, 3269–3293, doi:10.1175/2009MWR2827.1.

Eastin, M. D., W. M. Gray, and P. G. Black, 2005: Buoyancy of convective vertical motions in the inner core of intense hurricanes. Part I: General statistics. *Mon. Wea. Rev.*, **133**, 188–208, doi:10.1175/MWR-2848.1.

——, T. L. Gardner, M. C. Link, and K. C. Smith, 2012: Surface cold pools in the outer rainbands of Tropical Storm Hanna (2008) near landfall. *Mon. Wea. Rev.*, **140**, 471–491, doi:10.1175/MWR-D-11-00099.1.

Edwards, R. P., R. J. Krupar III, R. Warkentin, and S. Resnik, 2014: Modification of local roughness length by advancing storm surge in landfalling tropical cyclones. *11th Symp. on the Urban Environment*, Atlanta, GA, Amer. Meteor. Soc., 669. [Available online at https://ams.confex.com/ams/94Annual/webprogram/Paper238186.html.]

Franklin, J. L., M. L. Black, and K. Valde, 2003: GPS dropwindsonde wind profiles in hurricanes and their operational implications. *Wea. Forecasting*, **18**, 32–44, doi:10.1175/1520-0434(2003)018<0032:GDWPIH>2.0.CO;2.

Fujita, T. T., 1985: The downburst: Microburst and macroburst. SMRP Rep. 210, 122 pp. [NTIS PB-85-148880.]

——, 1992: Damage survey of Hurricane Andrew in South Florida. *Storm Data*, Vol. 34, 25–29.

Giammanco, I. M., J. L. Schroeder, and M. D. Powell, 2013: GPS dropwindsonde and WSR-88D observations of tropical cyclone vertical wind profiles and their characteristics. *Wea. Forecasting*, **28**, 77–99, doi:10.1175/WAF-D-11-00155.1.

Harper, B. A., J. D. Kepert, and J. D. Ginger, 2010: Guidelines for converting between various wind averaging periods in tropical cyclone conditions. WMO Rep. WMO/TD-1555, 64 pp. [Available online at https://www.wmo.int/pages/prog/www/tcp/documents/WMO_TD_1555_en.pdf.]

Houze, R. A., Jr., 1997: Stratiform precipitation in regions of convection: A meteorological paradox? *Bull. Amer. Meteor. Soc.*, **78**, 2179–2196, doi:10.1175/1520-0477(1997)078<2179:SPIROC>2.0.CO;2.

Jorgensen, D. P., 1984: Mesoscale and convective-scale characteristics of mature hurricanes. Part II. Inner core structure of Hurricane Allen (1980). *J. Atmos. Sci.*, **41**, 1287–1311, doi:10.1175/1520-0469(1984)041<1287:MACSCO>2.0.CO;2.

Kepert, J. D., 2001: The dynamics of boundary layer jets within the tropical cyclone core. Part I: Linear theory. *J. Atmos. Sci.*, **58**, 2469–2484, doi:10.1175/1520-0469(2001)058<2469:TDOBLJ>2.0.CO;2.

——, 2006a: Observed boundary layer wind structure and balance in the hurricane core. Part I: Hurricane Georges. *J. Atmos. Sci.*, **63**, 2169–2193, doi:10.1175/JAS3745.1.

——, 2006b: Observed boundary layer wind structure and balance in the hurricane core. Part II: Hurricane Mitch. *J. Atmos. Sci.*, **63**, 2194–2211, doi:10.1175/JAS3746.1.

——, and Y. Wang, 2001: The dynamics of boundary layer jets within the tropical cyclone core. Part II: Nonlinear enhancement. *J. Atmos. Sci.*, **58**, 2485–2501, doi:10.1175/1520-0469(2001)058<2485:TDOBLJ>2.0.CO;2.

Knupp, K. R., J. Walters, and M. Biggerstaff, 2006: Doppler profiler and radar observations of boundary layer variability during the landfall of Tropical Storm Gabrielle. *J. Atmos. Sci.*, **63**, 234–251, doi:10.1175/JAS3608.1.

Kosiba, K. A., and J. Wurman, 2014: Finescale dual-Doppler analysis of hurricane boundary layer structures in Hurricane Frances (2004) at landfall. *Mon. Wea. Rev.*, **142**, 1874–1891, doi:10.1175/MWR-D-13-00178.1.

——, ——, F. J. Masters, and P. Robinson, 2013: Mapping of near-surface winds in Hurricane Rita using finescale radar, anemometer, and land-use data. *Mon. Wea. Rev.*, **141**, 4337–4349, doi:10.1175/MWR-D-12-00350.1.

Krayer, W. R., and R. D. Marshall, 1992: Gust factors applied to hurricane winds. *Bull. Amer. Meteor. Soc.*, **73**, 613–617, doi:10.1175/1520-0477(1992)073<0613:GFATHW>2.0.CO;2.

Krupar, R. J., III, 2015: Improving surface wind estimates in tropical cyclones using WSR-88D derived wind profiles. Ph.D. dissertation, Texas Tech University, 200 pp. [Available online at https://ttu-ir.tdl.org/ttu-ir/bitstream/handle/2346/63660/KRUPAR-DISSERTATION-2015.pdf?sequence=1&isAllowed=y.]

Lopez, C., F. J. Masters, and K. Friedrich, 2011: Capture and characterization of wind-driven rain during tropical cyclones and supercell thunderstorms. *Proc. 13th Int. Conf. on Wind Engineering*, Amsterdam, Netherlands, International Association for Wind Engineering, 4 pp. [Available online at http://atoc.colorado.edu/~friedrik/PUBLICATIONS/2011_ICWE_Lopez.pdf.]

Lorsolo, S., J. L. Schroeder, P. Dodge, and F. D. Marks, 2008: An observational study of hurricane boundary layer small-scale coherent structures. *Mon. Wea. Rev.*, **136**, 2871–2893, doi:10.1175/2008MWR2273.1.

Mahrt, L., D. Vickers, J. Sun, N. O. Jensen, H. Jørgensen, E. Pardyjak, and H. Fernando, 2001: Determination of the surface drag coefficient. *Bound.-Layer Meteor.*, **99**, 249–276, doi:10.1023/A:1018915228170.

Marks, F. D., 1985: Evolution of the structure of precipitation in Hurricane Allen (1980). *Mon. Wea. Rev.*, **113**, 909–930, doi:10.1175/1520-0493(1985)113<0909:EOTSOP>2.0.CO;2.

——, R. A. Houze Jr., and J. F. Gamache, 1992: Dual-aircraft investigation of the inner core of Hurricane Norbert. Part I: Kinematic structure. *J. Atmos. Sci.*, **49**, 919–942, doi:10.1175/1520-0469(1992)049<0919:DAIOTI>2.0.CO;2.

——, P. G. Black, M. T. Montgomery, and R. W. Burpee, 2008: Structure of the eye and eyewall of Hurricane Hugo (1989). *Mon. Wea. Rev.*, **136**, 1237–1259, doi:10.1175/2007MWR2073.1.

Masters, F., F. Tieleman, and J.-A. Balderrama, 2010: Surface wind measurements in three Gulf Coast hurricanes of 2005. *J. Wind Eng. Ind. Aerodyn.*, **98**, 533–547, doi:10.1016/j.jweia.2010.04.003.

Miller, C., J.-A. Balderrama, and F. Masters, 2015: Aspects of observed gust factors in landfalling tropical cyclones: Gust components, terrain, and upstream fetch effects. *Bound.-Layer Meteor.*, **155**, 129–155, doi:10.1007/s10546-014-9989-0.

Molinari, J., J. Frank, and D. Vollaro, 2013: Convective bursts, downdraft cooling, and boundary layer recovery in a sheared tropical storm. *Mon. Wea. Rev.*, **141**, 1048–1060, doi:10.1175/MWR-D-12-00135.1.

Morrison, I., S. Businger, F. D. Marks, P. Dodge, and J. A. Businger, 2005: An observational case for the prevalence of roll vortices in the hurricane boundary layer. *J. Atmos. Sci.*, **62**, 2662–2673, doi:10.1175/JAS3508.1.

Paulsen, B. M., and J. L. Schroeder, 2005: An examination of tropical and extratropical gust factors and the associated wind speed histograms. *J. Appl. Meteor.*, **44**, 270–280, doi:10.1175/JAM2199.1.

Powell, M. D., 1990: Boundary layer structure and dynamics in outer hurricane rainbands. Part II: Downdraft modification and mixed layer recovery. *Mon. Wea. Rev.*, **118**, 918–938, doi:10.1175/1520-0493(1990)118<0918:BLSADI>2.0.CO;2.

——, P. Dodge, and M. L. Black, 1991: The landfall of Hurricane Hugo in the Carolinas: Surface wind distribution. *Wea. Forecasting*, **6**, 379–399, doi:10.1175/1520-0434(1991)006<0379:TLOHHI>2.0.CO;2.

——, S. H. Houston, and T. A. Reinhold, 1996: Hurricane Andrew's landfall in south Florida. Part I: Standardizing measurements for documentation of surface wind fields. *Wea. Forecasting*, **11**, 304–327, doi:10.1175/1520-0434(1996)011<0304:HALISF>2.0.CO;2.

——, ——, L. R. Amat, and N. Morisseau-Leroy, 1998: The HRD real-time hurricane wind analysis system. *J. Wind Eng. Ind. Aerodyn.*, **77–78**, 53–64, doi:10.1016/S0167-6105(98)00131-7.

——, P. J. Vickery, and T. A. Reinhold, 2003: Reduced drag coefficient for high wind speeds in tropical cyclones. *Nature*, **422**, 279–283, doi:10.1038/nature01481.

——, D. Bowman, D. Gilhousen, S. Murillo, N. Carrasco, and R. St. Fleur, 2004: Tropical cyclone winds at landfall: The ASOS–C-MAN wind exposure documentation project. *Bull. Amer. Meteor. Soc.*, **85**, 845–851, doi:10.1175/BAMS-85-6-845.

——, and Coauthors, 2010: Reconstruction of Hurricane Katrina's wind fields for storm surge and wave hindcasting. *Ocean Eng.*, **37**, 26–36, doi:10.1016/j.oceaneng.2009.08.014.

Schroeder, J. L., and D. A. Smith, 2003: Hurricane Bonnie wind flow characteristics as determined from WEMITE. *J. Wind Eng. Ind. Aerodyn.*, **91**, 767–789, doi:10.1016/S0167-6105(02)00475-0.

——, B. P. Edwards, and I. M. Giammanco, 2009: Observed tropical cyclone wind flow characteristics. *Wind Struct.*, **12**, 349–381, doi:10.12989/was.2009.12.4.349.

Schwendike, J., and J. D. Kepert, 2008: The boundary layer winds in Hurricanes Danielle (1998) and Isabel (2003). *Mon. Wea. Rev.*, **136**, 3168–3192, doi:10.1175/2007MWR2296.1.

Skwira, G. D., J. L. Schroeder, and R. E. Peterson, 2005: Surface observations of landfalling hurricane rainbands. *Mon. Wea. Rev.*, **133**, 454–465, doi:10.1175/MWR-2866.1.

Sparks, P. R., and Z. Huang, 2001: Gust factors and surface-to-gradient wind-speed ratios in tropical cyclones. *J. Wind Eng. Ind. Aerodyn.*, **89**, 1047–1058, doi:10.1016/S0167-6105(01)00098-8.

Stull, R. B., 1988: *An Introduction to Boundary Layer Meteorology*. Kluwer Academic, 666 pp.

Suomi, I., S.-E. Gryning, R. Floors, T. Vihma, and C. Fortelius, 2015: On the vertical structure of wind gusts. *Quart. J. Roy. Meteor. Soc.*, **141**, 1658–1670, doi:10.1002/qj.2468.

Vickery, P. J., and P. Skerlj, 2005: Hurricane gust factors revisited. *J. Struct. Eng.*, **131**, 825–832, doi:10.1061/(ASCE)0733-9445(2005)131:5(825).

Weiss, C. C., and J. L. Schroeder, 2008: StickNet: A new portable, rapidly deployable surface observation system. *Bull. Amer. Meteor. Soc.*, **89**, 1502–1503.

Wieringa, J., 1992: Updating the Davenport roughness classification. *J. Wind Eng. Ind. Aerodyn.*, **41**, 357–368, doi:10.1016/0167-6105(92)90434-C.

Willoughby, H. E., and M. B. Chelmow, 1982: Objective determination of hurricane tracks from aircraft observations. *Mon. Wea. Rev.*, **110**, 1298–1305, doi:10.1175/1520-0493(1982)110<1298:ODOHTF>2.0.CO;2.

Wurman, J., and J. Winslow, 1998: Intense sub-kilometer-scale boundary layer rolls observed in Hurricane Fran. *Science*, **280**, 555–557, doi:10.1126/science.280.5363.555.

Yu, B., A. G. Chowdhury, and F. J. Masters, 2008: Hurricane wind power spectra, cospectra, and integral length scales. *Bound.-Layer Meteor.*, **129**, 411–430, doi:10.1007/s10546-008-9316-8.

Yuter, S. E., and R. A. Houze Jr., 1995: Three-dimensional kinematic and microphysical evolution of Florida cumulonimbus. Part I: Spatial distribution of updrafts, downdrafts, and precipitation. *Mon. Wea. Rev.*, **123**, 1921–1940, doi:10.1175/1520-0493(1995)123<1921:TDKAME>2.0.CO;2.

Zhang, J. A., W. M. Drennan, P. G. Black, and J. R. French, 2009: Turbulence structure of the hurricane boundary layer between the outer rainbands. *J. Atmos. Sci.*, **66**, 2455–2467, doi:10.1175/2009JAS2954.1.

——, R. F. Rogers, D. S. Nolan, and F. D. Marks, 2011: On the characteristic height scales of the hurricane boundary layer. *Mon. Wea. Rev.*, **139**, 2523–2535, doi:10.1175/MWR-D-10-05017.1.